

Wright State University

CORE Scholar

[Browse all Theses and Dissertations](#)

[Theses and Dissertations](#)

2011

Functional Metabolomics' Enhances Assessment of Tissue Dysfunction as Demonstrated in a Rat Model of Sub-Acute D-Serine Exposure

Isaie Sibomana
Wright State University

Follow this and additional works at: https://corescholar.libraries.wright.edu/etd_all



Part of the [Molecular Biology Commons](#)

Repository Citation

Sibomana, Isaie, "Functional Metabolomics' Enhances Assessment of Tissue Dysfunction as Demonstrated in a Rat Model of Sub-Acute D-Serine Exposure" (2011). *Browse all Theses and Dissertations*. 519.

https://corescholar.libraries.wright.edu/etd_all/519

This Thesis is brought to you for free and open access by the Theses and Dissertations at CORE Scholar. It has been accepted for inclusion in Browse all Theses and Dissertations by an authorized administrator of CORE Scholar. For more information, please contact library-corescholar@wright.edu.

**'FUNCTIONAL METABOLOMICS' ENHANCES ASSESSMENT OF
TISSUE DYSFUNCTION AS DEMONSTRATED IN A RAT MODEL
OF SUB-ACUTE D-SERINE EXPOSURE**

A thesis submitted in partial fulfillment
of the requirements for the degree of
Master of Science

By

Isaie Sibomana

M.Phil., Entomology, University of Ghana, 2002

Agricultural Engineering, Polytechnic University of Bobo-
Dioulasso (Burkina Faso), 1999

B.S., National University of Rwanda, 1990

2011

Wright State University

WRIGHT STATE UNIVERSITY
SCHOOL OF GRADUATE STUDIES

December 6, 2011

I HEREBY RECOMMEND THAT THE
THESIS PREPARED UNDER MY SUPERVISION
BY Isaie Sibomana ENTITLED 'Functional Metabolomics
Enhances Assessment of Tissue Dysfunction as Demonstrated in a
Rat Model of Sub-Acute D-serine Exposure BE ACCEPTED IN
PARTIAL FULFILLMENT OF THE REQUIREMENTS
FOR THE DEGREE OF
Master of Science

Nicholas V. Reo, Ph.D.
Thesis Director

Steven J. Berberich, Ph.D.
Chair, Department of Biochemistry
and Molecular Biology

Committee on Final Examination

Nicholas V. Reo, Ph.D.

Michael L. Raymer, Ph.D.

Oleg Paliy, Ph.D.

Andrew Hsu, Ph.D.

Dean, Wright State University Graduate School

Abstract

Isaie Sibomana, M.S., Department of Biochemistry and Molecular Biology, Wright State University, 2011

'Functional Metabolomics' Enhances Assessment of Tissue Dysfunction as Demonstrated in a Rat Model of Sub-Acute D-serine Exposure

We describe a methodology that combines urinary metabolomics with a tissue-specific stressor administration to enhance assessment of tissue function. Kidney function in rats was mildly compromised with a sub-acute dose of D-serine and stressed with furosemide. NMR-based metabolomics analyses showed no detectable effects due to D-serine alone; but furosemide or D-serine + furosemide groups, classified separately from each other, and from control. Furosemide alone caused a *ca.* 2-fold increase in glucose, lactate, choline, and a 30% decrease in TCA intermediates ($p \leq 0.05$). D-serine suppressed these effects and produced a 1.7-fold increase in a *p*-phenolic acid-derivative of tyrosine (PAdY) relative to control ($p \leq 0.05$). The PAdY/tyrosine ratio increased 2-fold relative to rats given furosemide alone. D-serine effects were only detectable in furosemide-challenged rats, suggesting that minor disruption in kidney function, induced by low-level D-serine, is manifested by this functional metabolomics methodology. This technique may improve sensitivity for assessment of tissue function and disease.

Table of Contents

1. INTRODUCTION	1
1.1 Overview on NMR-based metabolomics	1
1.2 Challenges for NMR-based metabolomics approach.....	2
1.3 ‘Functional Metabolomics’ approach.....	3
1.3.1 Hypothesis and Strategy for Functional Metabolomics	3
1.3.2 Why D-serine in this study?	4
1.3.3 Why Furosemide administration in this study?	6
2. MATERIALS AND METHODS.....	9
2.1 Experimental Design	9
2.2 Sample Preparation	11
2.3 NMR Data Acquisition and Processing	11
2.4 Multivariate Data Analyses	14
2.5 Qualitative assessment of effects related to fasting and re-feeding	17
3. RESULTS	18
3.1 Metabolic response to fasting and re-feeding	18
3.2 Metabolic response to D-serine and furosemide treatments	24
4. DISCUSSION.....	40
4. 1 Fasting and furosemide treatment mediate an increase in urinary volume output.	40

4. 2 Fasting and re-feeding induce an alteration in urinary metabolite levels	41
4. 3 Low-dose D-serine effects are only observable in metabolically stressed kidney.	43
5. CONCLUSIONS.....	50
6. REFERENCES	51

List of Figures

Figure 1. Mechanism for D-serine toxicity	6
Figure 2. Chemical Structure of furosemide	8
Figure 3. Schematic diagram of the experimental design.	10
Figure 4. Steps involved in ¹ H NMR data processing and analyses	13
Figure 5. Urinary volume output across sampling times.	19
Figure 6. PCA model based on all groups at all time points.....	25
Figure 7. PCA model based on control and furosemide groups at 24 h.	26
Figure 8. PCA models based on control and treated groups at 48 h.	28
Figure 9. OPLS-DA models based on control and treated groups.....	31
Figure 10. Diagram depicting all the combinations of OPLS-DA models used in extracting the salient features classifying control and treated groups at 48h. ..	32
Figure 11. PCA scores plots modeling VeVe + VeFu + DsFu groups at 48 h using (A) salient bins that classify these groups and (B) all 267 spectral bins.	34
Figure 12. The tyrosine catabolism pathway	49

List of Tables

Table 1. Metabolite changes associated with fasting and re-feeding in control rats.	22
Table 2. Metabolite fold-change ratios for treated (VeFu or DsFu) vs. control groups. ..	37
Table 3. Urinary metabolite ratios for VeVe, VeFu, and DsFu groups at 48 h.	39

Acknowledgements

I would like to express my sincere heartfelt gratitude toward my advisor Dr. Nicholas V. Reo for his guidance, wisdom, treasured advices, patience and full support throughout this project. I greatly appreciate the tremendous help and friendly support received from the members of his NMR laboratory such as Andrew Neuforth, Deirdre Mahle and Daniel Homer. I am particularly grateful to Andrew Neuforth for his contribution in various ways to this project.

My utmost gratitude also goes to Dr. Michael L. Raymer for his smart advices and support that contributed to the success of this work. I sincerely acknowledge the essential role that the members of his laboratory played toward the successful completion of this project. My special thanks go to Eric Moyer and Dan Wlodarski for their direct involvement by providing tools that were needed for metabolite quantification in this project. I am also indebted to Dr. Paul E. Anderson for his brilliant ideas and support.

I am grateful to Dr. Nicholas J. DeRaso and Dr. David R. Mattie for their advices and unquestionable assistance toward the implementation of the experimental design such as urine sample collections etc. I am also thankful to Dr. Oleg Paliy for accepting to be a member of my thesis committee.

Finally, my warm thanks are expressed to my lovely wife, kids and brother-in-law for their full support while I was away from my house working on this project. I can never thank you enough for your unconditional love and attention.

1. INTRODUCTION

1.1 Overview on NMR-based metabolomics

Metabolomics (1, 2), which is also known as metabonomics (3, 4) or metabolic profiling (5) is defined as the “quantitative measurement of the time-related multiparametric metabolic response of living systems to pathophysiological stimuli or genetic modification” (3). NMR-based metabolomics has been used to associate an organism’s health status to its metabolite profile measured in biofluids (e.g., urine, blood, fecal and tissue extracts) or tissue biopsies. Coupled with multivariate data analyses, the ^1H NMR-based metabolomics approach is a fast, accurate and reproducible analytical technique for visualization of biochemical changes in biofluids or tissues (3, 6-12). This methodology involves correlating observed changes in metabolite levels to the biological effects related to physiological stimuli or genetic modification, toxicological, pathophysiological or environmental conditions. The use of ^1H NMR-based metabolomics technique has recently gained attention for direct application in preclinical, clinical, environmental and biomedical areas (4) due to several advantages that the technique offers such as rapidity and simplicity in sample preparation, high reproducibility and direct reflection of biological events among others (13). Studies have highlighted its potential for the successful identification and characterization of toxicity (14-25), metabolic pathways perturbed in various cancers (26-33), disease-related stages in chronic lymphocytic

leukemia (34), and other pathophysiological conditions (10, 35). The power of this technique is demonstrated for instance by its ability to detect the biochemical alterations induced by drug/chemical exposure and precisely localize the target organ based on the changes in metabolite concentrations observed from a peripheral sample such as urine or blood (11). In fact, metabolomics constitutes an important tool required to give an insight on the impact of various factors that affect the health status such as the genetic modifications, exposure to stimuli (e.g., noxious agents, stressors, nutrients, etc), toxicological, pathophysiological or environmental conditions (12).

1.2 Challenges for NMR-based metabolomics approach

Although the NMR-based metabolomics approach offers clear advantages in health assessment and monitoring over the use of traditional clinical assays, it still has not been widely implemented in clinical settings. One obstacle to clinical metabolomics approaches is the fact that the metabolite profile of various biofluids is influenced by numerous factors that may or may not be related to the biological processes of interest. These include genetics (36), gender, age, nutrition (12, 37-39), disease processes, environment, xenobiotics, (40, 41) and personal factors such as diet, exercise, and use of medications, alcohol, tobacco, etc. (7). This high diversity, especially in humans, produces a high “background noise” in metabolite profiles, which impedes data interpretation. Thus relating metabolite profiles to health and disease is a formidable task. Some of this variability can be minimized by controlling factors such as diet, or imposing strict exclusionary criteria for subjects (i.e., exclude smokers or medications), but this has been met with limited success due to numerous uncontrollable factors (42-

44). Other methods attempt to examine the influence of perturbing factors on metabolite profiles (7, 12, 45-47), but data are confounding and incomplete given the complexity of the problem. A more promising approach involves longitudinal studies, which have provided evidence that individual metabolic phenotypes may exist (48), and their detection through multiple sample collection combined with advanced statistical methods ((49), and reference therein) may provide a means to eliminate the daily ‘metabolomics noise’.

1.3 ‘Functional Metabolomics’ approach

Although several studies have successfully used NMR-based metabolomics to point out differences in metabolite profiles inherent to gender, aging, nutrition (12, 37-39), toxicity (14-16, 18-25, 43), diseases (10, 32, 34, 35) and other health-related issues, there are various factors associated with human health conditions that may affect the sensitivity of metabolomics assessment. Thus, to make this technique more useful, there is a need to implement a well-designed approach that can enhance its sensitivity, which is the basis of this study.

1.3.1 Hypothesis and Strategy for Functional Metabolomics

Herein we describe a different approach, dubbed *functional metabolomics*, towards improving the sensitivity of metabolomics for detection of biologically relevant effects. This methodology strives to increase the “signal-to-noise” ratio in metabolomics, which may potentially improve its usefulness to measure real and meaningful biological effects above the daily background variability. We hypothesize that the ability to detect

meaningful metabolite alterations, those related to tissue function/dysfunction, can be greatly enhanced by applying an organ-specific “metabolic challenge”. The tissue response under a metabolically stressed condition will reduce inter-animal variability, and augment our capability to detect biologically relevant changes in urinary metabolite profiles. Detection of abnormalities (i.e., tissue dysfunction due to chemical exposure or disease) will be enhanced when the stressor is applied. This approach is analogous to a glucose tolerance test to check for diabetes. Here, glucose is given as a body’s metabolic challenge and the body’s ability to clear the glucose from the blood reflects either normal or altered insulin sensitivity.

We tested this hypothesis in a rat model, using kidney as the target organ and furosemide, a diuretic drug, as an exogenous metabolic challenge (tissue stressor). Further, we compared normal healthy animals to animals that were exposed to a sub-acute dose of D-serine, a well-characterized nephrotoxin. This low-dose D-serine exposure was undetectable by standard urinary metabolomics analyses. But the mild kidney dysfunction in D-serine-treated animals was revealed under the furosemide-induced (kidney-stressed) condition. Theoretically, this functional metabolomics methodology could be extended (1) to evaluate tissues or organ systems other than kidney by developing tissue-targeted metabolic stressors, and (2) to detect tissue dysfunction due to disease as well as exposure to xenobiotics.

1.3.2 Why D-serine in this study?

D-serine is a well-known kidney toxicant that was used in this study at a sub-acute dose to mildly disrupt kidney function. Several intensive studies have described the

nature of its toxicity in rat models (20-22, 50-52). D-serine is specifically re-absorbed into the pars recta (or S3 straight segments) region of proximal tubules where the D-amino acid oxidase (D-AAO) enzyme is localized (53). Proximal tubular necrosis can develop as a result of excessive D-AAO enzymatic metabolism of D-serine, which can generate reactive oxygen species and lead to a decrease in the levels of renal glutathione (Figure 1) (54).

A study involving LEA/SENDAI rats that lack D-AAO enzyme highlighted the role of this enzyme in D-serine-induced nephrotoxicity as these rats were not affected by D-serine exposure when compared to their counterpart F344 rats which were characterized by excessive excretion of glucose and urine after being exposed to the same dose of D-serine (55). D-serine down-regulates various metabolic pathways such as the TCA cycle through inhibition of citrate synthase enzyme (56), resulting in depletion in citrate, α -ketoglutarate and succinate (22). D-serine has also been reported to have a negative effect on oxidative phosphorylation, ATP synthesis coupled electron transport, amino acid transport, metabolism of lipids, nucleotides, vitamins, carbohydrates and on oxidative stress response (57). Other studies have also indicated that it induces an increase in urinary excretion of glucose, lactate, acetate and alanine (22). The common biomarkers of D-serine toxicity observed with rat models include proteinuria, amino aciduria, glucosuria (Ganote *et al.*, 1974; Carone & Ganote, 1975). The sub-acute dose of D-serine used herein (60 mg/kg) was chosen based upon literature reports and preliminary studies in our laboratory. Williams, *et al.* (21) found no observable alterations in urinary metabolite profiles in Alderley Park rats exposed to 62.5 mg/kg D-serine. Additionally, studies in our laboratory (unpublished data) using Fischer-344 rats

showed no effects of D-serine at 50 mg/kg in comparison to 100 mg/kg, which was characterized by glucosuria, proteinuria and amino aciduria. Thus, a dose of 60 mg/kg D-serine was expected to be just below the threshold at which measureable effects can be observed and was used in this study. At an effective dose, the maximal D-serine-induced nephrotoxicity is observed within 24-48 h post exposure ((21); unpublished data from our laboratory).

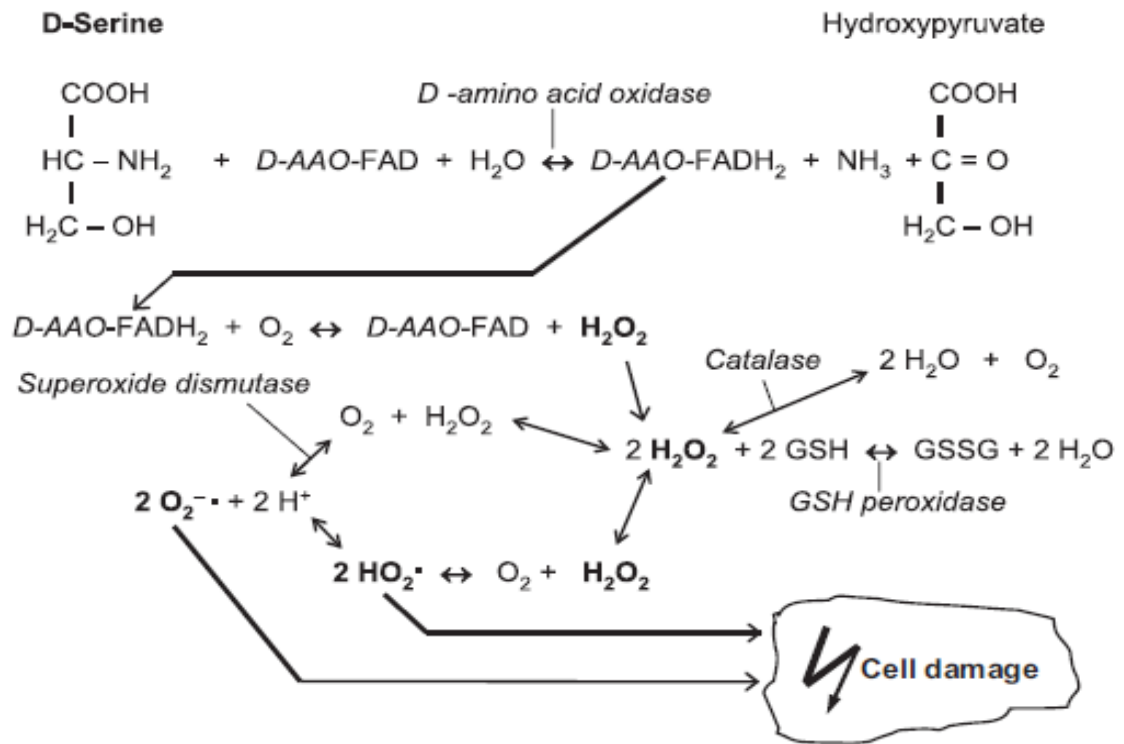


Figure 1. Mechanism for D-serine toxicity

1.3.3 Why Furosemide administration in this study?

Furosemide is a clinically used diuretic drug and was used here as a mild chemical stressor targeting the kidney. Figure 2 shows its chemical structure (58). Furosemide reversibly binds to $\text{Na}^+/\text{2Cl}^-/\text{K}^+$ co-transport proteins in the thick ascending

limb of the loop of Henle, reducing the reabsorption of the salt and water, resulting in a profound increase in urinary output (59-63). Other studies have suggested an extension of furosemide effect to the distal tubules (64, 65). Furosemide is also reported to confer renal protection by reducing oxygen requirement through the inhibition of the active NaCl transport (66, 67). By inducing an increase in tubular blood flow, furosemide can also drive a decrease in nephrotoxin concentrations (68).

The time at which furosemide was given to animals was made to coincide with 24 h post D-serine administration as our laboratory (unpublished data) and other studies (21, 52) have established that the maximum effect of D-serine toxicity is observable within 24-48 h of treatment. The dose of furosemide (10 mg/kg) was based upon studies showing maximal diuretic effectiveness in rats within 1 hour postdose (69, 70). Furosemide was expected to exert a minor pressure on kidney activity, thus helping to detect any weakness in kidney function. The use of furosemide in this study is analogous to the glucose tolerance test performed in diabetes screenings. As the glucose is given as the metabolic challenge and the body's ability to clear the glucose from the blood reflects to which extent the body is normally functioning. Furosemide was expected to expose the ability of kidney in handling a D-serine dose characterized as a non-harmful dose.

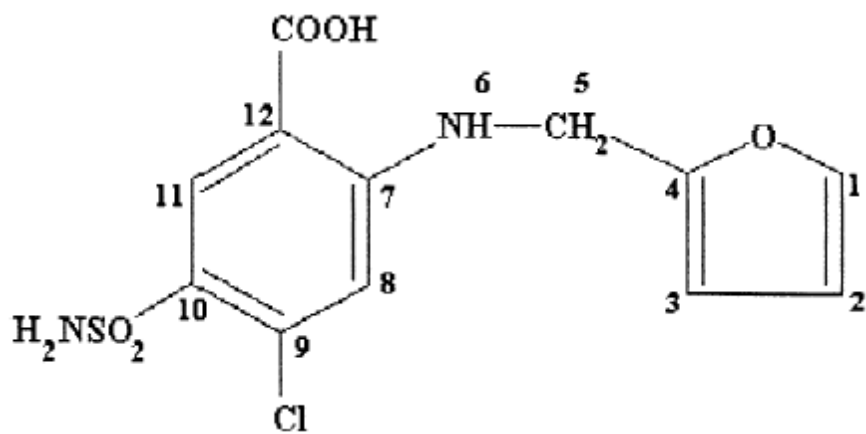


Figure 2. Chemical Structure of furosemide with corresponding proton numbering

2. MATERIALS AND METHODS

The protocols for handling laboratory animals were approved by the Wright-Patterson Institutional Animal Care and Use Committee (IACUC), and all animal experiments were conducted in accordance with federal guidelines. Furosemide was purchased from Webster Veterinary, Columbus, OH and D-serine was from Sigma-Aldrich. Both compounds were prepared in 0.9% sterile saline solution (vehicle).

Male Sprague-Dawley rats (200 – 225 g) were purchased from Charles Rivers Laboratories (Raleigh, NC) and were quarantined (3 days) and allowed to acclimate to housing conditions involving a 12 h light-dark cycle at 25 °C with *ad libitum* access to food and water. At 4 days prior to the start of the study, animals were randomly assigned to one of four experimental groups (N=12/group) and housed individually in metabolism cages.

2.1 Experimental Design

The experimental design involved two intraperitoneal (IP) injections (10 ml/kg) separated by 24 h, and all animals were also fasted during this 24 h period (Figure 3). We chose to fast animals in order to establish a more consistent metabolic state and minimize effects due to random feeding among animals; all animals were provided *ad libitum* access to water during the fasting period. Metabolism cages were fitted with 50

ml urine collection tubes containing 1 ml of 1% sodium azide, and maintained at 6–10 °C using I-Cups (Bioanalytical Systems, Inc., West Lafayette, IN). Three baseline urine samples were collected prior to the administration of dosing solutions (at -48, -24 and 0 h), and daily thereafter. All urine samples were stored at -80 °C until subsequent preparation for NMR analysis. On days involving treatments, urine was always collected prior to IP injection of animals. For the first injection at t=0, animals were given vehicle (Ve) or 60 mg/kg D-serine (Ds), while the second injection at 24 h involved vehicle or 10 mg/kg furosemide (Fu). The four experimental groups are designated by those treatments in which animals received vehicle alone (VeVe), furosemide alone (VeFu), D-serine alone (DsVe), or D-serine + furosemide (DsFu).

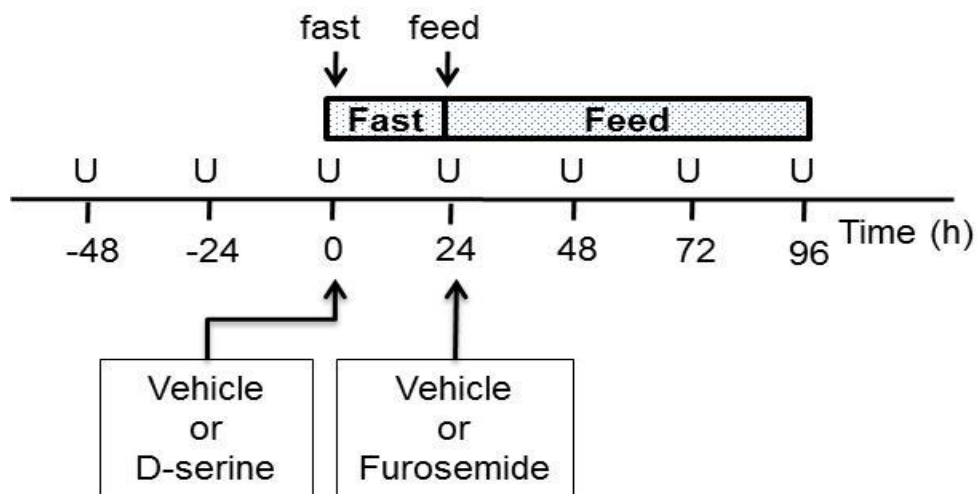


Figure 3. Schematic diagram of the experimental design depicting times of treatments (arrows) and urine collections (U). See text for details.

2.2 Sample Preparation

Frozen urine samples were thawed at 4 °C overnight. A 600 μ l aliquot of urine was then mixed with 300 μ l of phosphate buffer (0.2 M mono- and disodium phosphate; pH 7.4) and centrifuged at 13,000 rpm for 10 min to remove any precipitates. A 550 μ l aliquot of the supernatant was transferred to a 5 mm NMR tube and mixed with 150 μ l of 2,2',3,3'-tetra deuterio-trimethylsilylpropionic acid (TSP) in deuterium oxide (D_2O), adjusted to yield a final concentration of 2 mM. The TSP served as a chemical shift reference ($\delta = 0.00$ ppm) and D_2O provided a field-frequency lock for NMR data acquisition.

2.3 NMR Data Acquisition and Processing

All 1H NMR spectra were acquired using a Varian INOVA operating at 600 MHz and probe temperature of 25 °C. Water suppression was achieved using the first increment of a NOESY pulse sequence, which incorporated saturating irradiation at the water resonance frequency during a 2 s relaxation delay (pre-saturation) and again during a 50 ms mixing time. A total of 128 transients were collected per spectrum using an acquisition time of 4.0 s and inter-pulse delay of 11.05 s.

Steps involved in 1H NMR data processing and analyses are outlined in Figure 4. NMR data were processed using Varian software (VNMR 6.1c) employing exponential multiplication (producing line-broadening of 0.30 Hz), Fourier transformation, and phase correction. Spectra were then baseline corrected (flattened) in MATLAB (The Mathworks, Inc. Natick, MA; v. R2010b) using the Whittaker Smoother algorithm (with

lambda value of 200) on selected spectral noise regions (71, 72). Quantification of specific metabolite resonances was accomplished using an interactive spectral deconvolution algorithm in MATLAB adapted from our previously described methods (73). The deconvolution tool fits a defined spectral region using a combination of tunable baseline shapes (spline, v-shaped, linear, or constant) and a Gauss-Lorentz peak-fitting function. Integrated areas for peaks of interest are then output to a text file.

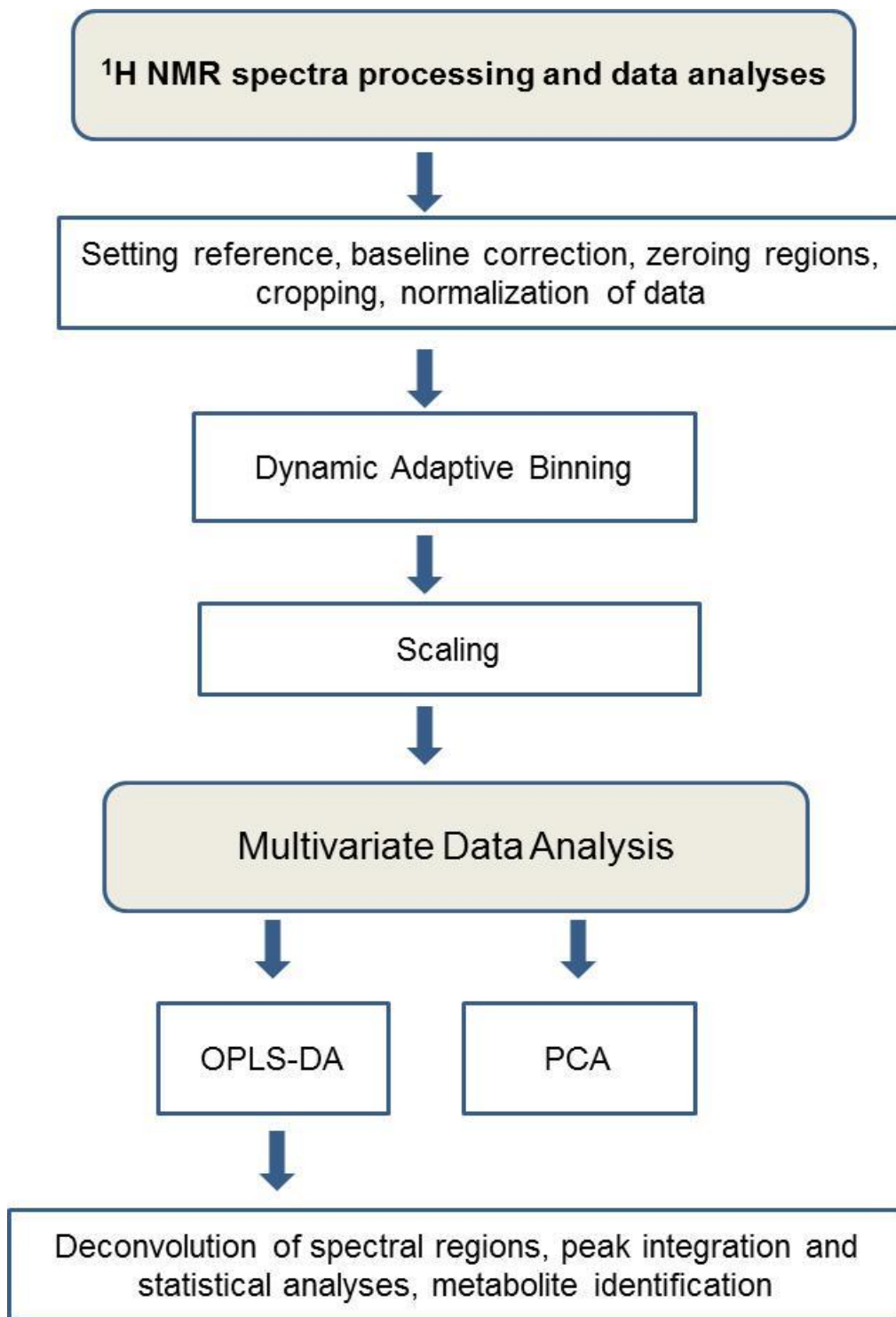


Figure 4. Steps involved in ^1H NMR data processing and analyses

Spectral processing for multivariate data analyses included removal of regions containing resonances from TSP (at 0.0 ppm), water (4.72 – 5.00 ppm), and urea (5.54 – 6.01 ppm). We also removed the spectral regions containing resonances from serine (3.82 – 3.86 and 3.92 – 4.01 ppm; (74) and preliminary studies in our laboratory), since D-serine was administered to some animals and was expected to be excreted in urine. The peak intensities for the remaining metabolite signals of each spectrum were then summed to a constant value (sum normalized). To reduce the dimensionality and mitigate peak misalignment, a dynamic programming-based adaptive binning technique was employed (73) using a minimum and maximum distance between peaks in a single bin of 0.001 and 0.04 ppm, respectively. Bin boundaries were then manually adjusted to further mitigate peak misalignment, and to keep known J-coupled multiplets within that same bin (e.g., doublets, triplets, etc). Data were then autoscaled using various datasets as reference depending upon which metabolic effects were being investigated (see below).

2.4 Multivariate Data Analyses

Multivariate data analyses were conducted on binned, scaled spectral data using MATLAB software. Binned NMR data were scaled to a chosen reference dataset by subtracting each bin value from the mean value for the corresponding bin in the reference data, then dividing this value by the standard deviation of the reference data (auto-scaling). The reference data for auto-scaling was chosen to emphasize specific effects (details are given in *Results*).

Unsupervised Analysis. Principal Component Analysis (PCA) provided a first-approach, unsupervised technique for data visualization. As previously described (75),

our analysis tools enable us to construct a PCA model based on specific experimental groups, and then apply the model-specific bin coefficients to other data groups to visualize these data relative to the existing model. To maximize visualization of specific responses, we modeled data based upon the nature of the effects being assessed. For instance, to visualize the effects (trajectory in PCA space) related to furosemide treatment, a PCA model comprising data from the furosemide-treated group (VeFu) and control group (VeVe) at all time points was constructed. Coefficients generated in this PCA model could then be applied to other groups (DsVe and DsFu) to create a trajectory into the latent vector space relative to the patterns created by the groups in the model (75). PCA scores plots were employed to help identify the time points of maximum effects for treatments.

Supervised Analysis. Orthogonal Projections onto Latent Structures Discriminant Analysis (OPLS-DA) was used to classify data and identify salient features that distinguish the various treatment and control groups. In order to apply OPLS-DA, spectral data are collected into a matrix of variables or bins (X) and a vector of categorical labels (Y), representing the effects. For these data, the categorical labels were treatment and time (e.g., DsFu, 48 h post-dose). These data were analyzed and modeled as follows: (1) determine a specific time point of interest (e.g., 48 h post-dose); (2) encode each treatment and corresponding control group as a two-group problem and analyze with OPLS (e.g., 1 = DsFu, 48 h post-dose; 2 = VeVe (control), 48 h post-vehicle); (3) using the model created for this specific two-group problem, project the remaining samples from other groups into the OPLS model.

Statistical Evaluation of OPLS Results. The OPLS model was evaluated on its predictive ability, using the Q^2 (coefficient of prediction) metric. Q^2 was calculated as follows:

$$Q^2 = 1 - \frac{PRESS}{SSY} = 1 - \frac{\sum_{i=1}^n (y_i - \hat{y}_i)^2}{\sum_{i=1}^n (y_i - \bar{y}_i)^2}$$

where PRESS is the Predicted RESidual Sum of Squares calculated as the residual e between the predicted and actual Y (class labels) during leave-one-out cross-validation, SSY is the Sum of Squares for y, \bar{y} is the y mean across all samples, and \hat{y}_i is the y value for sample i . As Q^2 approaches 1, the more predictive capability the model exhibits. A Q^2 value less than zero indicates that the model has no predictive power. A permutation test was performed to evaluate the significance of the Q^2 metric. The test involved repeatedly permuting the data labels and re-running the discrimination analysis, resulting in a distribution of the Q^2 scores (76). The Q^2 from the correctly labeled data is then compared to the distribution to determine the significance of the model at a specified alpha (set herein at $\alpha = 0.01$).

Variable selection (salient bins) from OPLS-DA was also statistically evaluated. The bin loadings, commonly referred to as coefficients, were compared to calculated null distributions in order to select for significance. The null distribution for each bin was determined by refitting the OPLS model to datasets in which each bin was independently and randomly permuted to remove any correlation between it and the control/treatment groups. The true OPLS model loading was then compared to the resulting null distribution of loadings, and values in the tail (greater than 99.5% or less

than 0.5% of the null distribution; corresponding to $\alpha = 0.01$) were assumed to contribute significantly to the model. The permutation was initially repeated 500 times for each bin and those near-significant loadings (greater than 92.5% or less than 7.5% of the null distribution; corresponding to $\alpha = 0.15$) were selected for 500 additional permutations (total 1000).

2.5 Qualitative assessment of effects related to fasting and re-feeding

The control group (VeVe) was used to assess the metabolite changes inherent to fasting and re-feeding. Effects of fasting and re-feeding were assessed by comparing the urinary spectral intensities obtained from urine samples collected at time 0 h (reference) to those collected at 24 h (post fasting) and 48 h (24 h post re-feeding) respectively. Data for the reference time point (0 h) and data for fasting or re-feeding were included in the supervised OPLS-DA (see details in the section on *multivariate analyses*) model to generate salient features (bins) that classify the two times. Then the NMR spectra from the time point of reference and those for fasting or re-feeding were superimposed using MATLAB software (The Mathworks, Inc. Natick, MA; v. R2010b). This assessment was conducted on sum normalized spectral data. Spectra for these two time points that were being investigated were identified by different colors. Then, their spectral intensities in each bin were qualitatively compared. The peak intensities for the time point of interest (fasting or re-feeding) was scored as decreasing or increasing relative to the referenced time (0 h).

3. RESULTS

3.1 Metabolic response to fasting and re-feeding

Urine samples were collected daily from 48 Sprague-Dawley rats (4 experimental groups with N=12/group) for a period of 7 days (see Fig. 3). Serial changes in the mean urinary volume outputs for each experimental group are shown in Figure 5. Urine output at predose times (-48, -24, and 0 h), and at 72 h and 96 h are similar among all groups. Fasting, however, produced a significant increase in urine output (observable at 24 h), which returned to baseline levels within 24 h of re-feeding (observable at 48 h). A two-way repeated measures ANOVA (treatment and time as factors) and Tukey posthoc test ($p \leq 0.05$) was used to analyze volume changes between predose (represented by the average of -48, -24, and 0 h data), 24 h and 48 h time points. Volume output for all groups at 24 h was significantly increased relative to predose ($p \leq 0.05$). This effect, due to fasting, has also been reported by others (77). For animals not receiving furosemide (VeVe and DsVe), urine output returned to baseline levels by 48 h (within 24 h of re-feeding). Animals dosed with furosemide (DsFu and VeFu), however, showed significantly higher urine output at 48 h (24 h post furosemide treatment) in comparison to the control group (VeVe) ($p \leq 0.05$). Thus furosemide was an effective diuretic drug at the dose used in this animal model.

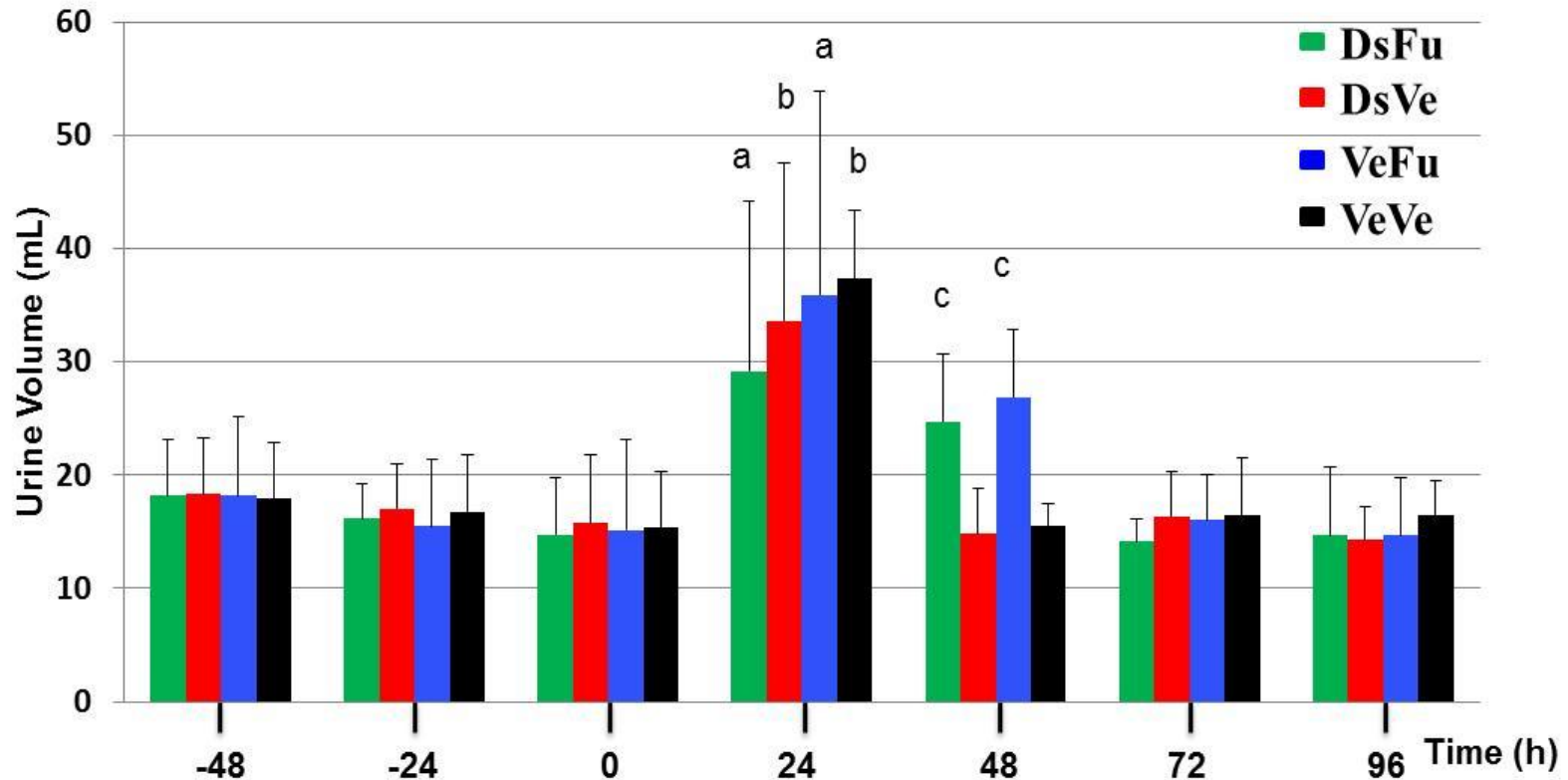


Figure 5. Changes in 24 h-urinary volume output (Mean \pm SD; N=12/group) from Sprague-Dawley rats during the experimental protocol diagramed in Figure 3. Data at predose (average of -48, -24, and 0 h time points), 24 h and 48 h were analyzed by a two-way repeated measures ANOVA and Tukey HSD posthoc test. Within-group significant differences ($p \leq 0.05$) are denoted by “a” (different from predose) and “b” (different from predose and 48 h). Groups that are significantly different from the control group (VeVe) at 48 h are denoted by “c” ($p \leq 0.05$).

Unsupervised PCA models depicted in Figures 6 and 7 indicate a common clustering of all the groups at 24 h post fasting. However, this clustering of groups was separate from the mapping positions at the pre-dose times, depicting the metabolite changes that are attributable to fasting conditions. The greatest separation in data was observed between pre- and post-fasting times (t=0 and t=24 h, respectively) as well as between 24 h and 48 h (24 h post re-feeding). These also were the periods within which the highest urinary outputs were collected. As the increase in urine volumes is translated into an excretion of diluted metabolites, the metabolic changes associated with fasting and furosemide treatment may be broader in scope and modest in magnitude.

To assess the effects of fasting and re-feeding on the metabolite changes, two OPLS-DA models were performed using the control (VeVe) data (Table 1). The first model evaluated the effects of fasting by comparing the data collected at time 0 h (prior to fasting) to data for the 24 h time point (post fasting) and the model was significant ($Q^2 = 0.93$; $\alpha = 0.01$; accuracy = 96). Impact of re-feeding on the metabolite alterations was assessed in a model that compared data obtained at 0 h (baseline) to those collected at 48 h (post re-feeding) and it was significant ($Q^2 = 0.95$; $\alpha = 0.01$; accuracy = 100). Metabolites in the significant bins that were generated by the two OPLS-DA models are listed in Table 1 along with information about their intensity changes. Our study has documented a considerable range of metabolites that are decreasing or increasing following the fasting or re-feeding periods (Table 1). The red arrow indicates an increase in the metabolite intensities while the black arrow depicts a decrease. Fewer metabolites (23 metabolites) were out of normal ranges within 24 h post-refeeding period as compared to metabolites (32 metabolites) that responded to the 24 h fasting period. Out

of 23 metabolites that were altered relative to the baseline, 20 of them were characterized by an increase. Similar effects of fasting and re-feeding were characterized by an increase of glycolytic products (pyruvate and lactate), amino acids (alanine and isoleucine/leucine), acetate, benzoate, allantoin, phenylacetyglycine and creatinine. TCA intermediates (citrate and α -ketoglutarate) and hippurate displayed a continuous decrease (during fasting and re-feeding). Some of the metabolites that were negatively affected by the fasting displayed an increase inherent to re-feeding. These were malonate, creatinine, methylguanidine, 3-hydroxyisobutyrate, trigonelline, urocanate, *trans*-Aconitate and homovanillate. Intensity levels of the amino acids such as lysine/arginine and glycine, glucose, fumarate, methylamine, dimethylamine, sarcosine, butaine, trimethyl amine oxide (TMAO), choline, taurine and pyridoxine were normalized within the 24 h of re-feeding. Although fasting did not have an effect on the urinary levels of formate, trimethylamine and thymidine, re-feeding induced their increase.

Table 1. Metabolite changes associated with fasting and re-feeding in control Sprague-Dawley rats (VeVe group).

Metabolite	Direction of changes relative to baseline (0 h)	
	post fasting (at 24 h)	post re-feeding (at 48 h)
<i>Glycolysis</i>		
Glucose	↑	-
Pyruvate	↑	↑
Lactate	↑	↑
<i>TCA intermediates</i>		
Citrate	↓	↓
α -ketoglutarate	↓	↓
Fumarate	↓	-
<i>Amino acids</i>		
Alanine	↑	↑
lysine/arginine	↑	-
isoleucine/leucine	↑	↑
Glycine	↑	-
<i>Others</i>		
Methylamine	↓	-
Dimethylamine	↓	-
Sarcosine	↓	-
Betaine	↓	-
TMAO	↓	-
Hippurate	↓	↓

Table 1 – *Continued*

Malonate	↓	↑
Creatine	↓	↑
Methylguanidine	↓	↑
3-hydroxyisobutyrate	↓	↑
Trigoneiline	↓	↑
Urocanate	↓	↑
<i>trans</i> -Aconitate	↓	↑
Homovanillate	↓	↑
Choline	↑	-
Acetate	↑	↑
Taurine	↑	-
Benzoate	↑	↑
Allanto in	↑	↑
Phenylacetyl glycine	↑	↑
Pyridoxine	↑	-
Creatinine	↑	↑
Formate	-	↑
Trimethylamine	-	↑
Thymidine	-	↑

↑ Increase

↓ Decrease

- No change

3.2 Metabolic response to D-serine and furosemide treatments

Figure 6 shows a PCA scores plot (PC1 vs PC2) that models all groups (VeVe, DsVe, VeFu, DsFu) at all time points (-48, -24, 0, 24, 48, 72, 96 h). Data were autoscaled using all groups at pre-dose times (-48, -24, 0 h) as reference. Trajectories across time are mainly due to fasting (at 24 h) and re-feeding (at 48 h) effects, but data return to the predose position by 96 h (data at 72 and 96 h are omitted in the plot for clarity). All groups respond equally to fasting as evidenced by a common clustering at 24 h. The control (VeVe) and DsVe groups display similar mapping position at all times, indicating no observable effect of D-serine treatment in the absence of furosemide. Interestingly, at 48 h slight differences are observed in mapping positions between groups, which presumably reflect changes in urinary metabolite profiles that are induced by furosemide and a combination of D-serine/furosemide treatments (VeFu and DsFu groups).

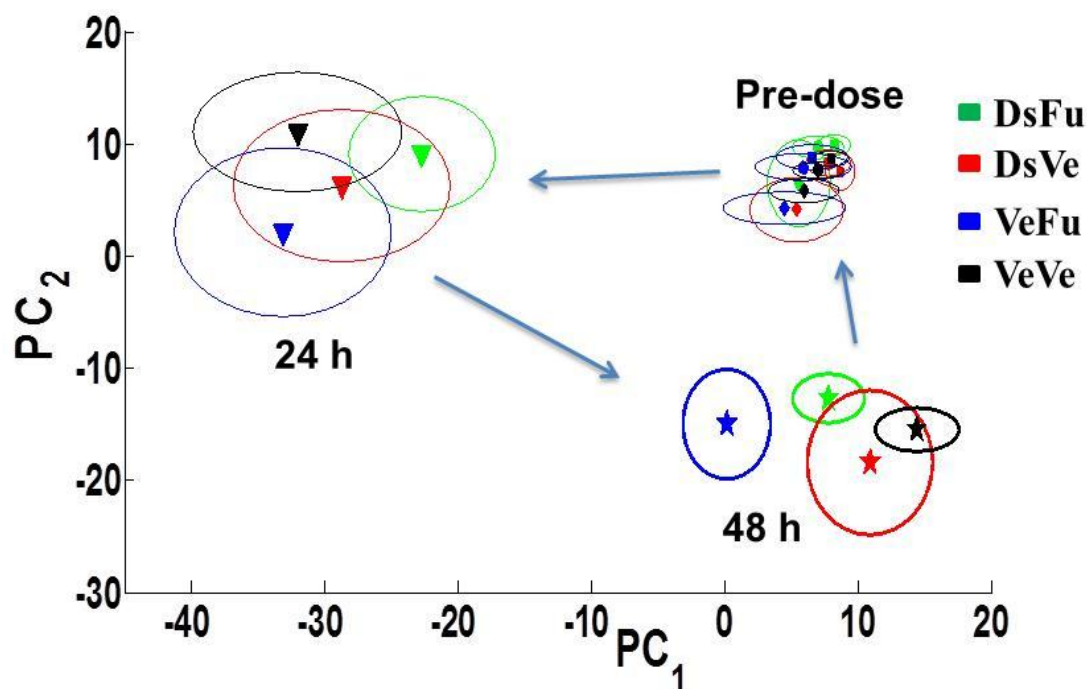


Figure 6. PCA scores plot (PC1 vs. PC2 representing 41% of total variance) based on rat urinary NMR spectra from functional metabolomics study. Symbols and ellipses are centroid mean \pm 2SE; arrows show trajectories across time. Data were autoscaled (see Methods) relative to all pre-dose time points (-48, -24, 0 h), and the PCA model includes all groups at all time points. Data at 72 h and 96 h are not shown for clarity but follow a trajectory towards the pre-dose times.

Although the D-serine/furosemide and furosemide-induced effects are observable at 48 h, they are not fully exposed by this PCA model due to the overwhelming impact of fasting/re-feeding animals. In order to suppress the impact of fasting and highlight the effects that are attributable to treatments, data were autoscaled relative to VeVe + VeFu groups at 24 h (corresponding to the time of maximum effects due to fasting and including only animals receiving vehicle solution; note: furosemide was administered after the 24 h urine collection). A PCA model based on these groups (VeVe + VeFu)

across all time points (autoscaled relative to 24 h) is shown in Figure 7. Data from DsVe and DsFu groups were superimposed in the plot using coefficients derived from the PCA model. Clustering of the groups at predose and 24 h times is apparent, similar to the results observed in Figure 6 and, as expected, suppressing the effects of fasting resulted in better separation between animals receiving furosemide *versus* vehicle (VeFu and DsFu *vs.* VeVe and DsVe) observed at 48 h. Moreover, the model does not display any difference in mapping positions between the control (VeVe) and DsVe groups, again indicating the lack of observable effects from D-serine treatment.

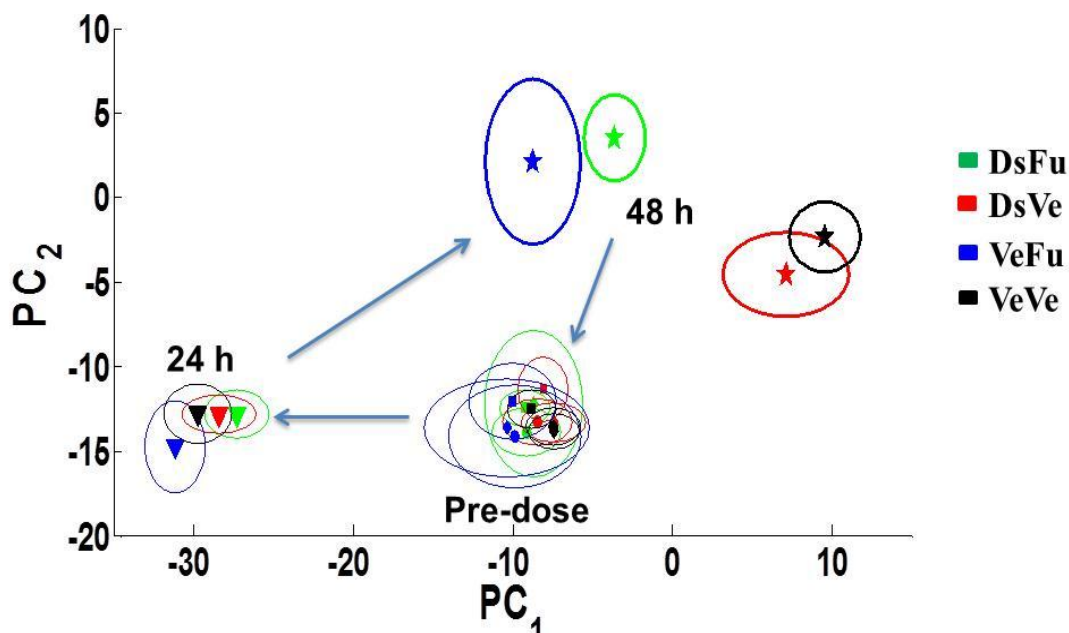


Figure 7. PCA scores plot (PC1 *vs.* PC2 representing 49% of total variance) based on rat urinary NMR spectra for VeVe + VeFu groups at all time points, with data autoscaled (see Methods) to these same groups at 24 h. Data from DsVe and DsFu groups were

superimposed in the plot using coefficients derived from the PCA model. Symbols and ellipses are centroid mean \pm 2SE; arrows show trajectories across time. Data at 72 h and 96 h are not shown for clarity but follow a trajectory towards the pre-dose times.

Effects due to D-serine and furosemide treatments should be apparent at 48 h, thus we used PCA to model these groups together with the control group (VeVe) at 48 h, and autoscaled these data relative to VeVe at 48 h to minimize effects due to re-feeding. Groups not included in the model were superimposed in the PCA scores plots (Figure 8) using the coefficients derived from the PCA model. Figure 8A and 8B show good separation between animals receiving furosemide *versus* vehicle along PC1 (VeFu and DsFu *vs.* VeVe and DsVe). Again the VeVe and DsVe groups overlap as expected, but the groups receiving furosemide alone *versus* a combination of D-serine + furosemide show an emerging separation at 48 h, particularly in Figure 8A.

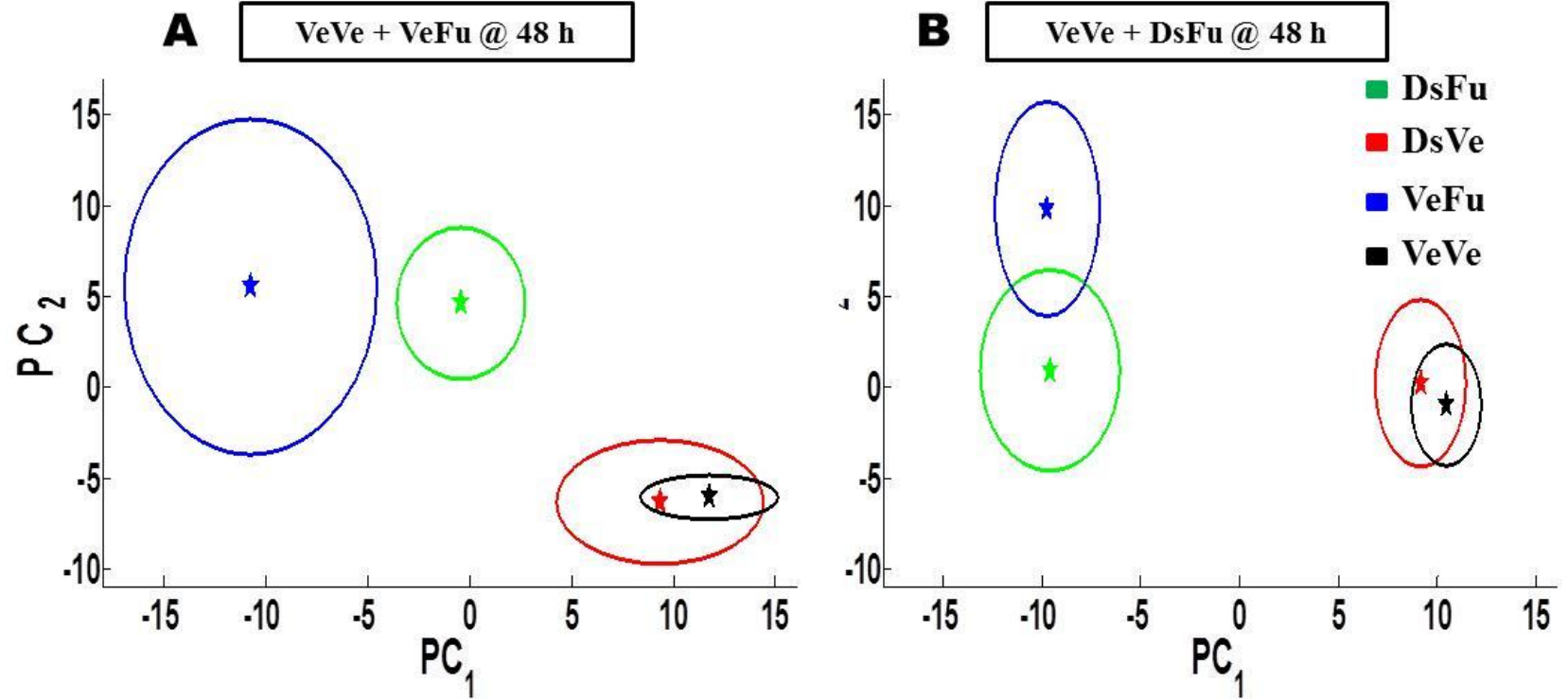


Figure 8. PCA scores plots modeling (A) VeVe + VeFu at 48 h (PC₁ vs. PC₂ representing 54% of variance), and (B) VeVe + DsFu at 48 h (PC₁ vs. PC₂ representing 39% of variance). Data for DsVe and DsFu at 48 h are superimposed in plot A, while data for DsVe and VeFu are superimposed in plot B using coefficients derived from the PCA models. All data were autoscaled (see Methods) relative to VeVe at 48 h, and symbols and ellipses are centroid mean ± 2SE.

OPLS discriminant analyses were conducted to evaluate the statistical significance and identify the salient features (spectral bins) that are associated with group classification at 48 h. The model significance was tested at $\alpha = 0.01$ and the results, displayed in Figure 9 (T vs. T Orthogonal plots), clearly show that animals receiving furosemide alone (VeFu) or D-serine + furosemide (DsFu) are significantly different from vehicle-treated controls (VeVe) (Fig. 9A and 9B). Indeed, the Q^2 values were ≥ 0.90 and the predictability accuracy for both models was 100% (leave-one-out cross validation). A total of 69 and 43 significant bins ($\alpha = 0.01$) were derived from VeVe *vs.* VeFu and VeVe *vs.* DsFu OPLS-DA models, respectively. An OPLS-DA for VeFu *vs.* DsFu at 48 h also yielded a significant result ($Q^2 = 0.44$; Accuracy = 100%) and generated 23 salient bins responsible for group classification (Fig. 9C). In a further analysis, we tested for correlation between the coefficients for these 23 significant bins found by OPLS-DA (Fig. 9C) and the loadings for principal component 1 from the PCA displayed in Fig. 5A, which showed a slight separation between VeFu and DsFu groups. Interestingly, Spearman's Rank Correlation showed these coefficients to be highly correlated (Spearman $|\rho| = 0.7194$; $p = 0.0001$) indicating that the unsupervised PCA and supervised OPLS-DA models are finding similar features to classify the effects of furosemide alone (VeFu) and a combination of D-serine + furosemide (DsFu). In each of the OPLS model plots shown in Figure 9, we superimposed data from the other groups not included in the model. As expected, VeVe and DsVe were clustered together similar to the PCA results. Additionally, an OPLS-DA for VeVe *vs.* DsVe was not significant ($Q^2 = 0.012$; $p = 0.01$), confirming that no significant effects from D-serine treatment alone were observable.

All the significant bins derived from the three OPLS-DA models (Fig. 9A, 9B and 9C) are shown in a Venn diagram (Fig. 9D) to illustrate the number of common and unique features derived from these models. Figure 10 depicts all the combinations of OPLS-DA models used in the extraction of the salient features that classify the VeVe, VeFu and DsFu groups. The analyses that classify and separate VeFu from VeVe (Fig. 9A) and DsFu from VeVe (Fig. 9B) yield 86 distinct bins, 26 of these are shared (identical bins) between the two models (Fig. 10). Presumably, these 86 bins are important for the classification of VeFu, DsFu and VeVe. Therefore, we conducted analyses similar to those presented in Figure 8, but used only these 86 significant bins as input to PCA. These PCA scores plots (data not shown) appear similar to those in Figure 8, which used all 267 spectral bins in the PCA models. Focusing on the clustering observed for VeFu and DsFu at 48 h, with an aim towards determining which bins are responsible for group classification, we again conducted OPLS-DA. An OPLS-DA model for VeFu *vs.* DsFu at 48 h using this limited set of 86 bins (OPLS scores plot not shown) is statistically significant ($Q^2 = 0.51$; accuracy = 96%) and yields 23 significant bins [shown in Fig. 10 as (B)] when the model significance is tested at $\alpha = 0.01$. Ten of these 23 bins are common (identical) to a set of bins that are derived from the same model, but using all 267 spectral bins [shown in Fig. 10 as (A)]. In other words, each of the two models (OPLS using 267 bins and OPLS using 86 bins as input) generates 13 unique features in addition to 10 shared features, yielding a total of 36 bins that drive the separation of VeFu and DsFu at 48 h (Fig. 10).

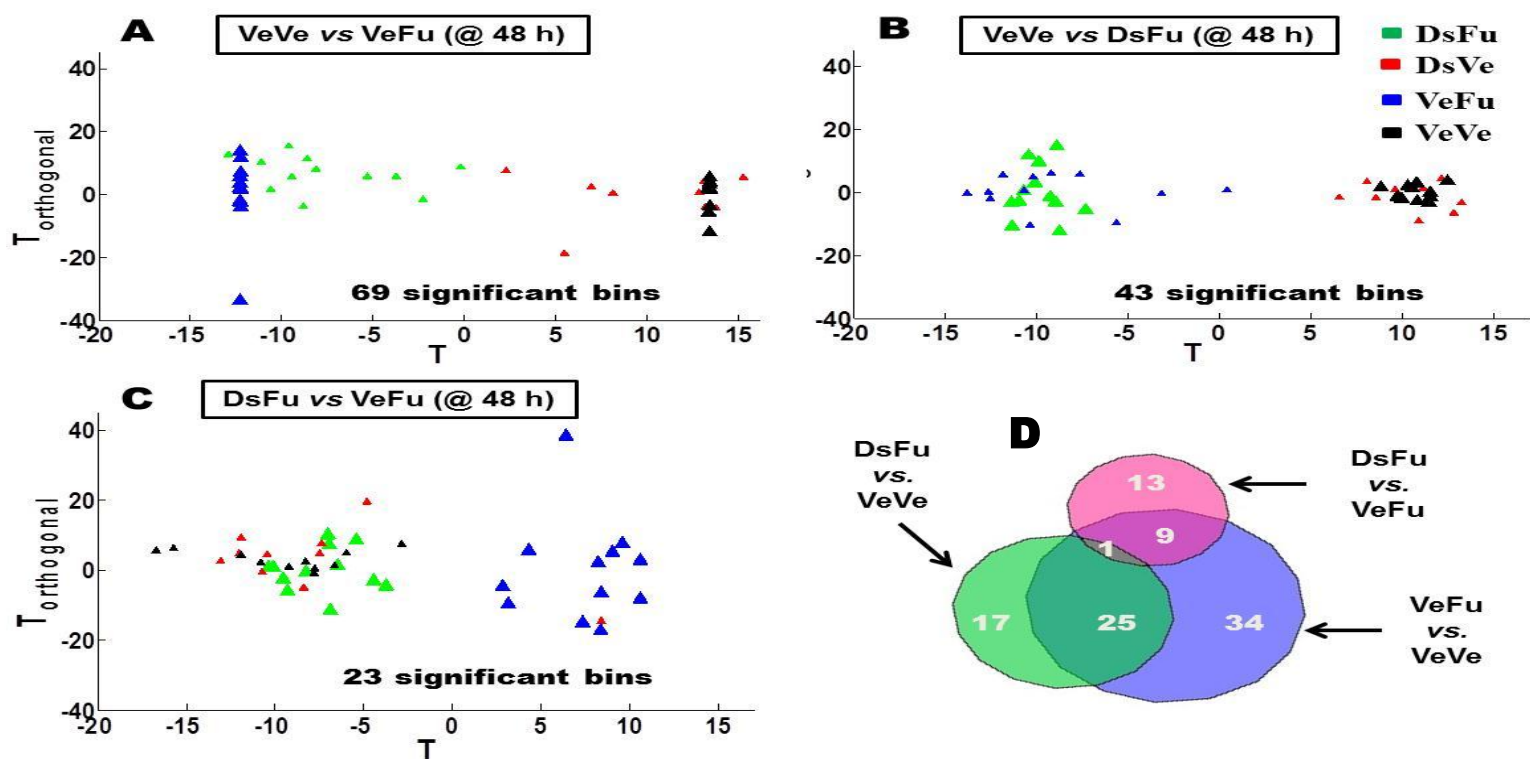


Figure 9. OPLS-DA models using rat urinary NMR spectra at 48 h with all data autoscaled to the control group (VeVe) at 48 h. (A) VeVe vs. VeFu ($Q^2 = 0.95$); (B) VeVe vs. DsFu ($Q^2 = 0.90$); and (C) DsFu vs. VeFu, ($Q^2 = 0.44$). Models A, B, and C are all statistically significant (test $\alpha = 0.01$; see Methods) and yield an accuracy of 100% (leave-one-out validation). Large symbols depict data from the modeled groups, while other groups superimposed in the model are shown in smaller symbols. The number of significant bins determined by the OPLS-DA model ($\alpha = 0.01$; see Methods) is indicated in each plot, and also displayed in a Venn Diagram (D).

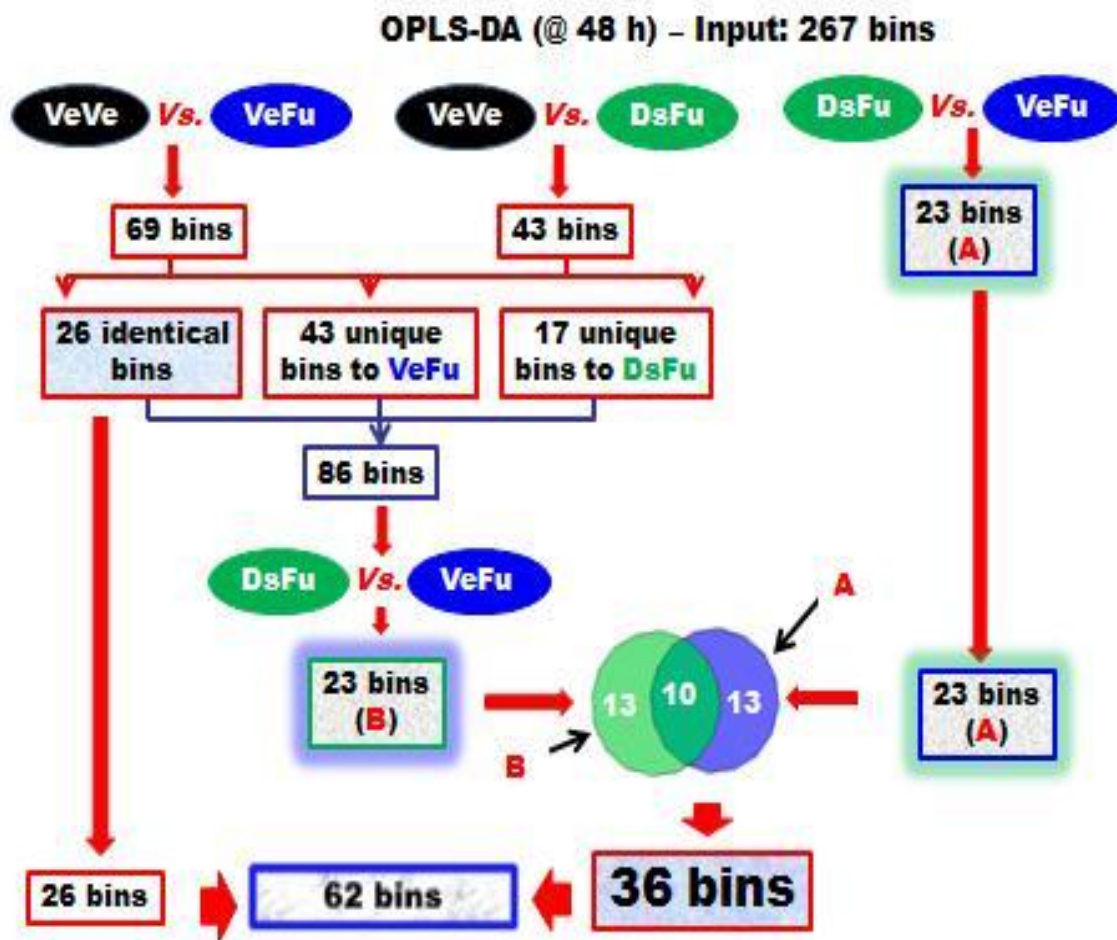


Figure 10. Diagram that depicts all the combinations of OPLS-DA models used in the extraction of the salient features that classify the control (VeVe), furosemide (VeFu) and D-serine + furosemide (DsFu) groups at 48 h.

Taken together, we find a total of 26 bins that are important for classifying VeFu and DsFu groups separately from vehicle control (VeVe) and an additional 36 features that are important for separating VeFu and DsFu groups at 48 h (see Fig. 10). Figure 11 shows PCA scores plots (PC1 vs PC2) based on a combination of all these features (26 + 36 = 62 bins; Fig. 11 A) and a total of 267 bins (Fig. 11 B). The PCA models include

VeVe + VeFu + DsFu at 48 h. The model constructed using 62 bins (Fig. 11 A) shows a clear distinction between VeVe, VeFu and DsFu groups. But when the DsVe group is superimposed in this model, these data overlap with the control group (VeVe). Thus there is a lack of observable effects from D-serine treatment alone, but in combination with furosemide distinct metabolic changes are observable that appear to be associated with 36 features. These 36 features may represent the salient urinary metabolite changes that reflect mild kidney dysfunction induced by exposure to low-dose D-serine. A comparison between the PCA scores plot shown in Figure 11 A to the PCA scores plot generated using all the 267 spectral bins (Fig. 11 B) indicates that a clear classification of the groups is obtained when the PCA model is based on a selection of 62 bins.

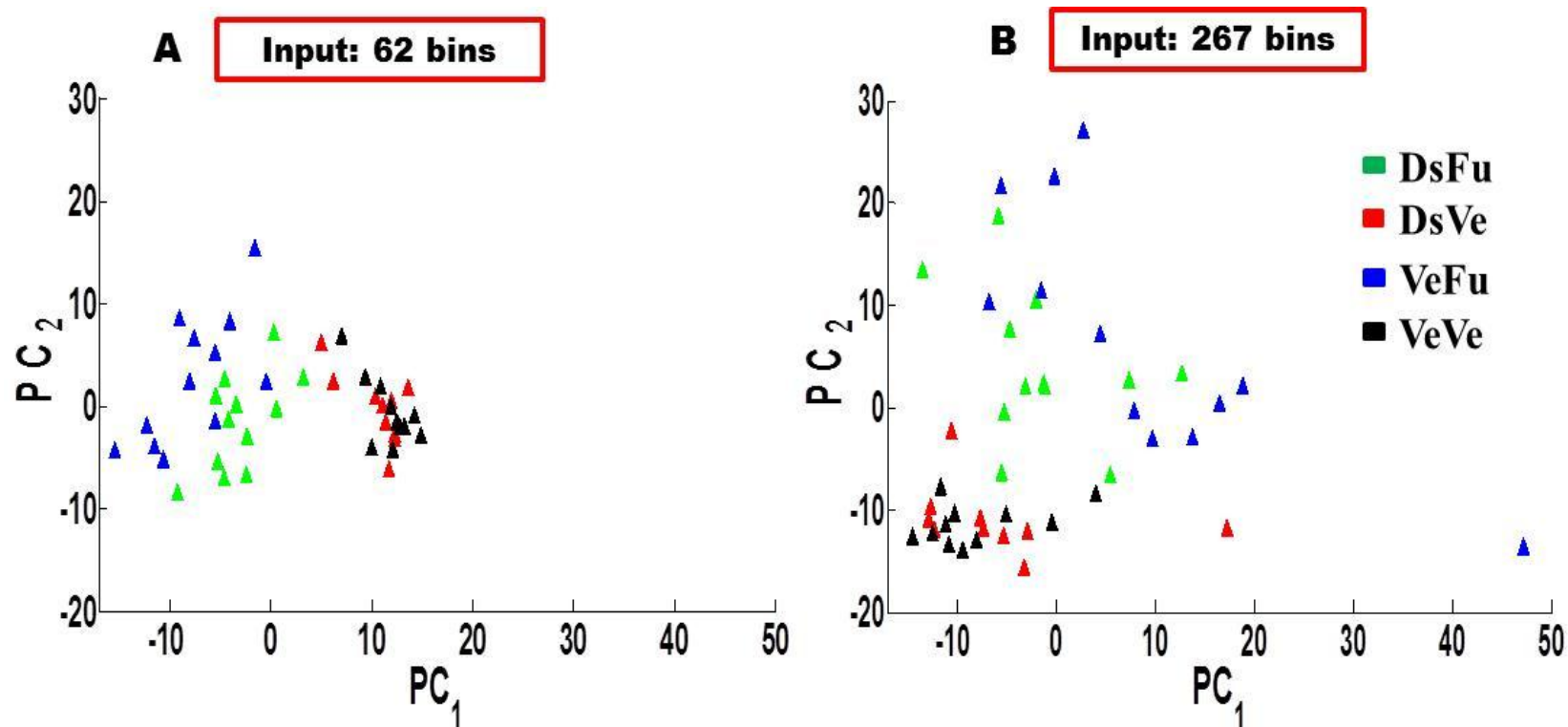


Figure 11. PCA scores plots modeling VeVe + VeFu + DsFu groups at 48 h with data autoscaled (see Methods) relative to VeVe at 48 h. (A) the PCA model uses a total of 62 bins selected by OPLS-DA (see text for details; PC₁ vs. PC₂ representing 59 % of total variance). (B) the PCA model uses all 267 spectral bins (PC₁ vs. PC₂ representing 43 % of total variance). Data from the DsVe group are superimposed in both plots using coefficients derived from the PCA models.

NMR spectral regions identified as significant by OPLS-DA were compared between experimental groups, and specific resonances were assigned to metabolites with the aid of literature, on-line databases (HMDB, <http://www.hmdb.ca/>), and Chenomx NMR Suite software (Edmonton, Alberta, CA). We analyzed the 36 significant bins derived from the OPLS-DA that emphasize the effects of D-serine observable in the presence of furosemide (VeFu *vs.* DsFu at 48 h). From these 36 bins we assigned 11 unique independent metabolites (some bins contained redundant information since multiple peaks were detected from the same metabolite) plus one additional signal that could not be identified. These 12 metabolite signals were quantified (integrated peak areas) using a spectral deconvolution/peak-fitting algorithm (see *Methods*). It is important to note that, because of the sum normalization procedure (see *Methods*), metabolite intensities are represented as a fraction of the total urinary metabolite pool in each sample. Table 2 displays these metabolite data expressed as a ratio of the treatment group (VeFu or DsFu) relative to control (VeVe) at 48 h. Table 2 also differentiates those data determined to be statistically significant by OPLS-DA for specific treatment *vs.* control groups, and those found to be significant when analyzed by peak integration and t-test (superscripts *a* and *b*, respectively). Relative to the control group (VeVe), furosemide treatment alone (VeFu) caused a *ca.* 2-fold increase in lactate, glucose, and choline, and a 30% decrease in citrate. These effects appear to be mitigated in the group exposed to D-serine prior to furosemide (DsFu) and, instead, this group shows a 1.7-fold increase (relative to VeVe) in a doublet signal at 6.83 ppm, which is characteristic of aromatic protons on a *para*-substituted phenol. This metabolite is likely to be a *p*-phenolic acid derivative of tyrosine such as 4-hydroxyphenylpropionic acid (desaminotyrosine), 4-

hydroxyphenylpyruvic acid (HPPA), or 4-hydroxyphenyllactic acid (HPLA). Desaminotyrosine seems an unlikely candidate since its source is microbial (gut microbial metabolism of tyrosine). Figure 12 shows the tyrosine metabolism pathway that generates the HPPA and HPLA compounds. These compounds are produced in kidney by transamination of tyrosine via tyrosine aminotransferase to yield HPPA, which can be reduced to HPLA by 4-hydroxyphenyllactate dehydrogenase. Others have also observed these metabolites in NMR spectra of rat urine under experimental conditions involving perturbations to the tyrosine catabolism pathway (20, 78). We could not unequivocally assign this metabolite since resonances from its aliphatic protons were obscured in densely populated regions of the spectrum. Therefore, we will refer to this metabolite as a *p*-phenolic acid derivative of tyrosine (PAdY).

Table 2. Changes in 12 urinary metabolites (U, unidentified) identified from 36 significant bins (some metabolites yielded signals in multiple bins) derived from OPLS-DA for comparisons between experimental groups at 48 h (see text for details). Values are reported as a fold-change ratio for treated (VeFu or DsFu) *versus* control (VeVe) groups. Peak multiplicities are indicated as: s, singlet; d, doublet; dd, double of doublet; t, triplet. Standard rules for propagation of errors were used to determine the \pm SE for calculated ratios.

Metabolite	Chemical Shift in ppm	Fold Change (Mean \pm SE)	
		VeFu/VeVe ratio	DsFu/VeVe Ratio
Lactate	1.33 (d)	2.2 \pm 0.6 ^{a, b}	1.2 \pm 0.2 ^a
Glucose	4.66 (d)	1.7 \pm 0.3 ^{a, b}	1.3 \pm 0.2 ^a
Choline	3.20 (s)	1.6 \pm 0.2 ^{a, b}	1.3 \pm 0.1 ^{a, b}
Tyrosine	3.16 (d)	1.2 \pm 0.1 ^a	1.1 \pm 0.1 ^a
PAdY ¹	6.83 (d)	0.9 \pm 0.2 ^a	1.7 \pm 0.3 ^b
Phenylacetyl-glycine	7.36 (t)	0.9 \pm 0.1 ^a	1.2 \pm 0.2 ^a
Homovanillate	6.76 (dd)	0.9 \pm 0.1 ^a	1.1 \pm 0.1 ^a
Unknown	7.46 (s)	0.9 \pm 0.1 ^a	0.9 \pm 0.1
Citrate	2.55 (d)	0.7 \pm 0.1 ^{a, b}	1.0 \pm 0.1
Dimethylglycine	2.93 (s)	0.7 \pm 0.2 ^a	0.8 \pm 0.2
Tryptophan	7.22 (t)	0.7 \pm 0.1 ^a	0.8 \pm 0.1 ^a
histidine + N,N-methylhistidine ¹	7.07 – 7.05	0.7 \pm 0.1 ^a	0.9 \pm 0.1

¹ A *p*-phenolic acid derivative of tyrosine (see text for details).

^a Significant bins from OPLS-DA for each specific treatment group *vs.* control ($Q^2 \geq 0.90$; $p \leq 0.01$).

^b Significant difference in treated *vs.* control for quantified metabolite signal (*t*-test, $p \leq 0.05$).

We also measured metabolite ratios within each urine sample for the VeVe, VeFu, and DsFu groups at 48 h (Table 3). We focused on those metabolites deemed important via OPLS-DA procedures and based ratios relative to the urinary creatinine level, or between metabolites that share a common pathway (e.g., homovanillate/tyrosine; PAdY/tyrosine; glycine + dimethylglycine/choline). In general, amino acids (represented as: tyrosine + tryptophan + histidine + N,N-methylhistidine) are decreased in the VeFu and DsFu groups relative to the vehicle control group (VeVe). Furosemide alone (VeFu) also caused a decrease in the citrate/creatinine ratio relative to the VeVe group. Therefore, we chose to measure other TCA (tricarboxylic acid cycle) metabolites that could be identified in the spectra including α -ketoglutarate (2.45 ppm), succinate (2.41 ppm), and fumarate (6.53 ppm). The sum of these TCA intermediates (citrate + α -ketoglutarate + succinate + fumarate) expressed as a ratio to creatinine was also significantly decreased in the VeFu group relative to control. These metabolite ratios, however, were unaffected in the DsFu group. The sum of glycine and dimethylglycine expressed as a ratio to choline (glycine + dimethylglycine/choline) was also reduced in the VeFu group relative to control (VeVe), but this ratio was again unaffected in the DsFu group. Interestingly, the PAdY/tyrosine ratio in the DsFu group was not different from the control (VeVe) value, but was 2-fold higher in comparison to the VeFu.

Table 3. Urinary metabolite ratios (Mean \pm SE) for VeVe, VeFu, and DsFu experimental groups measured at 48 h.

Metabolite Ratios	VeVe	VeFu	DsFu
lactate / creatinine	0.5 \pm 0.1	0.8 \pm 0.2	0.4 \pm 0.1
glucose / creatinine	0.3 \pm < 0.1	0.3 \pm < 0.1	0.3 \pm 0.1
phenylacetyl glycine / creatinine	0.2 \pm < 0.1	0.2 \pm < 0.1	0.2 \pm < 0.1
citrate / creatinine	3.2 \pm 0.2	1.7 \pm 0.2 ^a	2.4 \pm 0.3
TCA intermediates / creatinine ¹	21.2 \pm 3.0	9.9 \pm 1.3 ^a	19.3 \pm 3.1 ^b
Relevant amino acids / creatinine ²	0.5 \pm 0.1	0.3 \pm < 0.1 ^a	0.3 \pm < 0.1 ^a
glycine + dimethylglycine / choline	8.3 \pm 1.0	5.5 \pm 0.7 ^a	6.9 \pm 1.0
homovanillate / tyrosine	1.1 \pm 0.1	0.8 \pm 0.1	1.0 \pm 0.1
PAdY / tyrosine	0.3 \pm < 0.1	0.2 \pm < 0.1	0.4 \pm < 0.1 ^b

¹ TCA intermediates = citrate + α -ketoglutarate + succinate + fumarate.

² Relevant amino acids = tyrosine + tryptophan + histidine + N,N-methylhistidine.

^a Significantly different from the control (VeVe) group (*t*-test and Bonferroni correction; $p \leq 0.05$).

^b Significantly different from the VeFu group (*t*-test and Bonferroni correction; $p \leq 0.05$).

4. DISCUSSION

This study combined a tissue-targeted metabolic challenge (stressor) and NMR-based metabolomics to investigate whether this approach could enhance sensitivity to detect tissue dysfunction. We used an animal model and targeted kidney with a diuretic stressor (furosemide) and induced mild tissue dysfunction with a known kidney toxicant (D-serine). The experimental protocol also included a 24-h fasting period in an attempt to reduce baseline variability in urinary metabolite profiles. Since the main focus of this study was not to assess the effects of fasting/re-feeding, we did not elaborate on these effects. Thus, we are reporting here simply the results on the qualitative assessment of effects related to fasting and re-feeding.

4. 1 Fasting and furosemide treatment mediate an increase in urinary volume output

Fasting and re-feeding animals induced significant metabolic effects, which nearly masked our capability to detect changes due to treatments. As seen in Figure 5, fasting also caused a significant increase in urinary volume output, which is consistent with previous reports in Sprague-Dawley rats (77, 79). A 2.4-fold increase in urine volumes was observable in the samples collected from fasted rats relative to the baseline samples. A 2-fold increase in urine volume for overnight (16 h) fasted Sprague-Dawley rats has also been documented (77). The mechanism for this fasting-induced urine

increase is well established and associated with a decrease in renal aquaporin proteins, and imbalance in the regulation of water reabsorption (79, 80).

As expected, furosemide treatment also caused a transient increase in urinary output at 24 h postdose (t=48 h in Fig. 5), with levels returning to baseline by the next urine collection time (t=72 in Fig. 5). The diuretic nature, metabolism and molecular basis of furosemide have been well characterized (61, 63-65, 70, 81, 82). The target and mechanism of these effects involves reversible binding of furosemide to luminal $\text{Na}^+/\text{2Cl}^-/\text{K}^+$ symporters in the thick ascending limb of the loop of Henle (59-63). Another portion of the nephron, the proximal tubules, is the target of D-serine nephrotoxicity.

4. 2 Fasting and re-feeding induce an alteration in urinary metabolite levels

Fasting has been found to be associated with down-regulation of the renal water channel (aquaporins), thus resulting in a decrease in water reabsorption (79). This decrease in water re-uptake can explain an increase in urine volumes we observed with the fasted rats. The current study performed a qualitative assessment of the effects related to fasting and re-feeding. The study documented a considerable range of metabolite changes due to fasting and re-feeding. Fasting induced an increase in urinary excretion of glucose, pyruvate, lactate and amino acids such as alanine, lysine/arginine, isoleucine/leucine and glycine. An increase in urinary excretion of other metabolites such as choline, acetate, taurine, benzoate, allantoin, phenylacetyl glycine, pyridoxine and creatinine was also observed following the 24 h fasting period. Several studies have reported a wide range of metabolic changes that are associated with fasting (77, 83-89).

Boedigheimer and colleagues (89) have identified fasting as one of the most significant sources of variation in gene expression levels. Most recently, Robertson and coworkers (77) showed that fasting of rats produced changes in most of the urine metabolites detected in NMR spectral profiles, although the magnitude of these changes was relatively small. Other studies have reported a fasting-induced down-regulation of several proteins involved in glycolysis in male Wistar rats (90) and mice (88). Lenaerts *et al.* (2006) have documented changes in protein expression levels and amino acid metabolism that were inherent to 24 h fasting effects. They observed a down-regulation of initiation translation factors, thus suggesting an inhibition of protein synthesis (91). This could probably explain the increase of amino acid excretion we observed in our study. We also noted that fasting induced a decrease in certain TCA intermediates such as citrate, α -ketoglutarate and fumarate and a set of 14 other metabolites as listed in Table 1. A decrease in TCA intermediates following fasting has also been documented by other studies (77, 90). Robertson and coworkers (77) have identified alteration in several genes that encode the TCA cycle enzymes including a decrease of citrate synthase. Currently, the fasting-induced decrease in TCA cycle intermediates is not well understood. Many of these TCA intermediates and other metabolites such as acetate, creatinine, hippurate, lactate, taurine, trimethyl amine oxide (TMAO) are among the metabolite that have been characterized as “usual suspects” as they frequently change in response to any treatment (22). Fewer metabolites (23 metabolites) were out of normal ranges within 24 h post-refeeding. Most of them (20 metabolites) were characterized by an increase in intensity. Only three metabolites (citrate, α -ketoglutarate and hippurate) displayed a continuous decrease. The differences in normalization of metabolites after a period of fasting may

reflect the differential enzymatic adaptations to re-feeding. Studies have demonstrated that the rates of glucose metabolism are enhanced during re-feeding (92-95). However, the energy restoration may depend upon carbohydrate absorption since it has been demonstrated that an inhibition of carbohydrate absorption in male Sprague-Dawley rats correlates with a delay in the energy accumulation following re-feeding (96).

4.3 Low-dose D-serine effects are only observable in metabolically stressed kidney

In this study, D-serine was used to mildly compromise kidney function. Studies have shown that the maximum effect of D-serine toxicity as manifested in rat urinary metabolite profiles is observable within 24 – 48 h post-exposure at doses ≥ 100 mg/kg, with non-observable effects for doses ≤ 62.5 mg/kg ((21), and unpublished data from our laboratory). Based upon these previous studies, the selected sub-acute D-serine dose (60 mg/kg) in the current study was not expected to cause any observable effects in normal healthy rats. This outcome was confirmed. D-serine treatment alone (DsVe group) showed no significant changes in urinary metabolite profiles in comparison to corresponding controls (VeVe group) when examined by PCA or OPLS-DA (Figs. 6-10).

The goal of this study was to test whether this functional metabolomics approach can enhance the sensitivity of NMR-based metabolomics to detect slight changes in kidney function that may only be detectable under a metabolically stressed condition. Thus we focused on extracting the urinary metabolite changes that are unique in classifying the VeFu and DsFu groups. Interestingly, PCA and OPLS-DA models generated distinct mapping positions for the VeVe, VeFu, and DsFu groups at the 48 h time point. This time corresponds to 48 h post D-serine and 24 h post furosemide

treatment. These differences in mapping positions support our hypothesis that D-serine-induced temporal metabolite changes are observable only when the kidney is metabolically stressed. Most importantly, we find that the significant features (bins) leading to separation between the VeFu and DsFu groups, as derived from a supervised OPLS-DA, are highly correlated with the loadings from an unsupervised PCA (Spearman's Rank; $p = 0.0001$). Thus supervised and unsupervised analyses found similar variables that are important for group classification. Through a step-wise progression of multivariate data analyses, we identified 36 significant bins derived from the OPLS-DA models that appear to be associated with D-serine-mediated disruption of kidney function. A detailed spectral analysis assigned these changes to 12 metabolites that are influenced by treatments (furosemide alone or D-serine + furosemide). In normal functioning kidney, furosemide caused a significant increase in glucose, lactate, and choline, and a decrease in citrate (Table 2; VeFu/VeVe ratio). But in rats exposed to D-serine in combination with the metabolic stress associated with furosemide (DsFu group), all of these metabolite changes were abolished, with the exception of choline (Table 2; DsFu/VeVe ratio). These results suggest that D-serine disrupted, or mitigated, the normal response to furosemide. The glycine+dimethylglycine/choline ratio was also significantly reduced by furosemide treatment (Table 3), an effect not observed in the DsFu group (these metabolites share a common pathway).

With regard to effects on glucose, others have also reported a furosemide-induced increase in glucose excretion in rats (97-100), mice (101), human (98, 102), and cell-free preparations obtained from rabbit kidney (98). Jacobs, *et al.* (100) have suggested that this effect of furosemide may involve inhibition of glucose transport through a direct

inactivation of its carrier proteins. Whatever the cause of this effect on glucose excretion, it is mitigated by low-dose D-serine exposure (i.e., not observed in the DsFu group).

Urinary metabolite ratios were also calculated for glucose, lactate, citrate, TCA intermediates, and several amino acids (termed relevant amino acids) that were found to be important (by OPLS-DA) for detection of any functional abnormalities of kidney induced by D-serine. These metabolite ratios were measured relative to creatinine, as urinary creatinine clearance has been regarded as an indicator of renal injury (*103, 104*), and creatinine was not among the significant features found by our OPLS-DA models. Citrate and TCA intermediates, whether measured relative to the total urinary metabolite pool (Table 2) or expressed relative to creatinine (Table 3), were decreased by furosemide treatment alone but were unaffected in the DsFu group. Thus this furosemide-associated metabolic effect appears to be mitigated by D-serine (observable only when the kidney is metabolically stressed by furosemide). Although lactate and glucose were increased by furosemide when expressed as a fraction of the total urinary metabolite pool, the lactate/creatinine and glucose/creatinine ratios were not different from controls. This prompted us to measure the stability of creatinine within these experimental groups. Indeed, treatment caused a significant increase in creatinine relative to controls (VeFu/VeVe = 1.3 ± 0.1 and DsFu/VeVe = 1.5 ± 0.2 ; Mean \pm SE, $p \leq 0.001$), but these changes in creatinine were not found to be a significant feature for OPLS-DA group classification. Reports regarding creatinine clearance in patients receiving furosemide treatment vary (*66, 68, 105*), and creatinine has been listed among the “usual suspects” that can frequently change in response to xenobiotics (*4*). Nonetheless, it is instructive to consider these data, particularly the TCA intermediate/creatinine ratio, which is

significantly reduced in the VeFu group relative to VeVe or DsFu. These results emphasize the importance of the effects observed for citrate and TCA intermediates, as these metabolites are not affected in the DsFu group even though creatinine levels significantly rise in this same group. Thus D-serine exposure impacts urinary excretion of TCA intermediates — an effect that is only observable when the kidney is metabolically challenged with furosemide. These results are interesting in light of the effects of D-serine nephrotoxicity observed at higher doses (≥ 100 mg/kg) (21), which include increased urinary excretion of glucose and lactate, and decreases in TCA intermediates (similar to that seen here with furosemide treatment alone). Thus the metabolite perturbations expected with high-dose D-serine alone (toxic dose) or furosemide alone, are suppressed in rats receiving low-dose D-serine followed by furosemide challenge. In contrast, the perturbation on creatinine excretion induced by furosemide (e.g., increased urinary excretion), was not affected by prior administration of low-dose D-serine. Thus some metabolic processes were perturbed while others were not, which may be related to differences in the specific sites of action for D-serine and furosemide in the nephron. Regardless, these metabolite perturbations reflect abnormalities in kidney function imposed by low-dose D-serine, which are only observable when the kidney is stressed by furosemide.

A significant and unique metabolic effect observed in the DsFu group relates to the excretion of a *p*-phenolic acid derivative of tyrosine (PAdY), presumably HPPA and/or HPLA (Fig. 12). These metabolites of tyrosine degradation have been observed previously in NMR spectra of rat urine following inhibition of 4-hydroxyphenylpyruvate dioxygenase (20, 78), the second enzyme in the tyrosine catabolism pathway that

converts HPPA to homogentisate. Although the PAdY metabolite might also be desaminotyrosine, we believe this is unlikely since it is produced via deamination of tyrosine occurring only in gut microbes. Regardless of its origin, a significant increase in urinary excretion of the PAdY metabolite was only observed in rats exposed to D-serine and then challenged with furosemide to stress the kidney. The DsFu group showed a 1.7-fold increase in PAdY relative to controls (Table 2), and the PAdY/tyrosine ratio was 2-fold higher in the DsFu group relative to the VeFu group (Table 3). Urinary excretion of tyrosine and PAdY in rats receiving D-serine alone was not different in comparison to vehicle controls (DsVe/VeVe ratio = 1.3 ± 0.2 and 1.1 ± 0.2 for tyrosine and PAdY, respectively, and the PAdY/tyrosine ratio = 0.2 ± 0.03 and 0.3 ± 0.04 for the DsVe and VeVe groups, respectively; no significant difference between groups, $p \leq 0.05$, t-test). Thus, furosemide alone or D-serine alone did not affect tyrosine or PAdY urinary excretion. These results provide evidence that the plasma levels of tyrosine and PAdY are unaffected by these treatments (albeit we did not measure plasma metabolites), suggesting that the differences seen in the DsFu group reflect altered kidney function with regard to tyrosine metabolism, or the excretion of tyrosine and its derivatives. We speculate that low-dose D-serine induces a minor insult to renal tubules that, when combined with the additional stress imposed by furosemide, perturbs the clearance of phenolic acids. Interestingly, Williams, *et al.* (20) reported a perturbation in the normal handling of phenolic acids following severe renal damage induced by 250 mg/kg D-serine in rats, which was only observed in the presence of an enzyme inhibitor of tyrosine metabolism in kidney. In their study, inhibition of 4-hydroxyphenylpyruvate dioxygenase caused increased production and urinary clearance of phenolic acids (HPPA and HPLA)

in normal functioning kidney. But following D-serine-induced kidney damage, rats instead displayed tyrosinuria with minimal excretion of phenolic acids. Thus it is possible that some perturbation in the normal handling and excretion of phenolic acids also occurs at a sub-acute dose of D-serine, but this effect is only manifested under an additional metabolic stress to the kidney (e.g., furosemide). This may represent a unique effect associated with tubular damage, which would not have been observed without the functional metabolomics methodology described herein. Further studies would be of interest to investigate whether the use of phenolic acids as a kidney stressor would be a more useful and sensitive means to assess kidney function/dysfunction.

One might argue that the effects observed here are unique because they reflect the combined treatment of D-serine plus furosemide; however, we believe this is unlikely since the tissue accumulation, injury, and clearance of D-serine is rapid and occurs prior to administration of furosemide 24 h later. William, *et al.* (21) reported that maximal levels of serine were present in the rat kidney within 30 min of dosing and the first signs of tissue injury appear at about 1 h. Additionally, 17% of the administered dose was excreted within the first 8 h, and rats showed recovery from D-serine toxicity beginning at 24 h. Others have also reported rapid urinary clearance of D-serine in rats, with 28% excreted within 24 h (106). Thus, we believe that the effects observed in our study reflect abnormalities in kidney function induced by low-dose D-serine, prior to administration of furosemide. Another matter to consider is possible bias of our experimental design, which used an optimal timing for D-serine and furosemide dosing. In other words, the maximal effect of D-serine was expected to occur at 24 h postdose, which was chosen to coincide with the furosemide challenge. This likely influenced the results since D-serine-related

effects at this dose are temporal. But this may not be a critical factor that compromises the utility of the methodology if it is used to screen for persistent tissue abnormalities. Further studies are necessary to investigate the relationship between tissue function and the timing of the metabolic challenge.

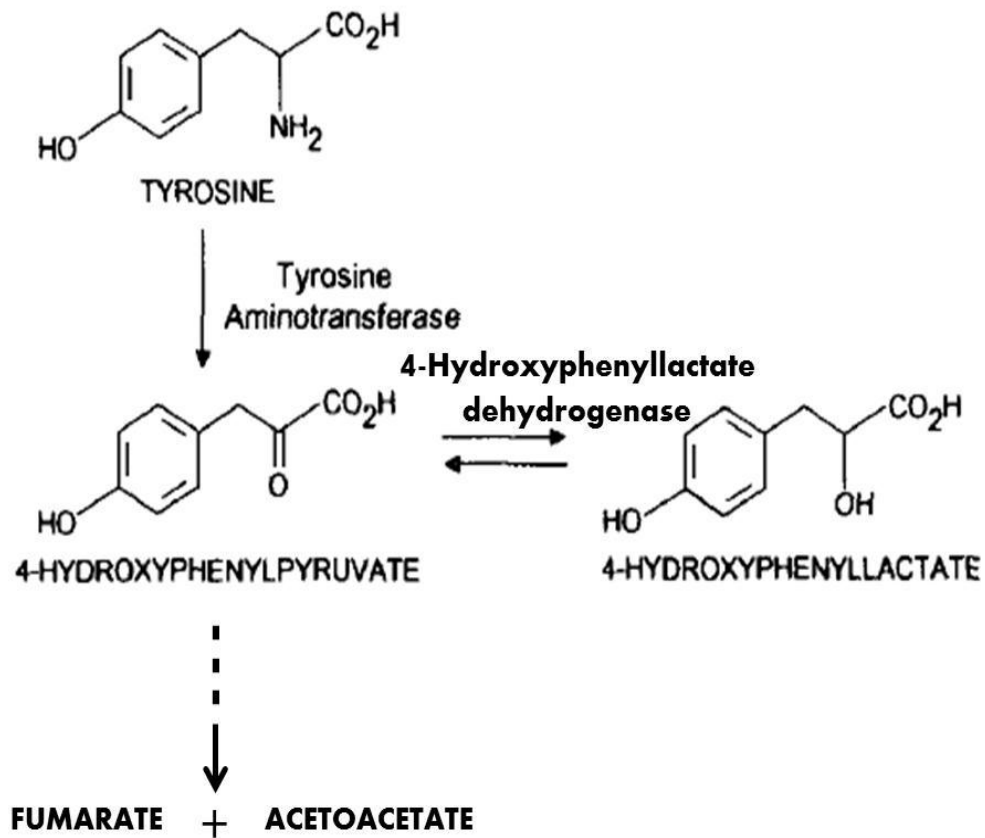


Figure 12. The tyrosine catabolism pathway

5. CONCLUSIONS

By combining a kidney-targeted metabolic challenge (tissue stressor) with urinary metabolomics analyses, we demonstrated enhanced sensitivity for detection of functional abnormalities in kidney that may be attributed to low-dose D-serine exposure. In summary, D-serine mitigated effects of furosemide on urinary excretion of glucose, lactate, and TCA intermediates. And D-serine caused a unique effect on tyrosine metabolism that was not observable in the absence of the stress imposed by furosemide. Although this functional metabolomics approach was limited to kidney, and used a very specific means to compromise kidney function (exposure to a nephrotoxin), our results are encouraging and can potentially be extended to other organ systems and functional abnormalities (i.e., disease pathophysiologies).

6. REFERENCES

1. Fiehn, O., Kloska, S., and Altmann, T. (2001) Integrated studies on plant biology using multiparallel techniques, *Current opinion in Biotechnology* 12, 82-86.
2. Tweeddale, H., Notley-McRobb, L., and Ferenci, T. (1998) Effect of slow growth on metabolism of *Escherichia coli*, as revealed by global metabolite pool ('metabolome') analysis, *Journal of Bacteriology* 180, 5109-5116.
3. Nicholson, J. K., Lindon, J. C., and Holmes, E. (1999) 'Metabonomics': understanding the metabolic response of living systems to pathophysiological stimuli via multivariate statistical analysis of biological NMR spectroscopic data, *Xenobiotica* 29, 1181-1189.
4. Robertson, D. G. (2005) Metabonomics in toxicology: a review, *Toxicological sciences* 85, 809-822.
5. Trethewey, R. N., Krotzsy, A. J., and Willmitzer, L. (1999) Metabolic profiling: Rosetta stone for genomics? , *Current opinion in Plant Biology* 2, 83-85.
6. Lindon, J. C., Holmes, E., and Nicholson, J. K. (2003) So what is the deal with the metabolomics? , *Analytical Chemistry* 75, 385A-391A.

7. Bollard, M. E., Stanley, E. G., Lindon, J. C., Nicholson, J. K., and Holmes, E. (2005) NMR-based metabolomics approaches for evaluating physiological influences on biofluid composition, *NMR in Biomedicine* 18, 143-162.
8. Lindon, J. C., Nicholson, J. K., Holmes, E., and Everett, J. R. (2000) Metabolomics: metabolic processes studied by NMR spectroscopy of biofluids, *Concepts in Magnetic resonance* 12, 289-300.
9. Nicholson, J. K., and Wilson, I. D. (1989) High resolution proton NMR spectroscopy of biological fluids, *Progress in Nuclear Magnetic Resonance Spectroscopy*, 449-501.
10. Xu, J., Zhang, J., Dong, J., Cai, S., Yang, J., and Chen, Z. (2009) Metabolomics studies and intact hepatic and renal cortical tissues from diabetic db/db mice using high-resolution magic-angle spinning ¹H NMR spectroscopy, *Analytical and Bioanalytical Chemistry* 393, 1657-1668.
11. Robertson, D. G., Reily, M. D., Sigler, R. E., Wells, D. F., Paterson, D. A., and Braden, T. K. (2000) Metabonomics: Evaluation of nuclear magnetic resonance (NMR) and pattern recognition technology for rapid in Vivo screening of liver and kidney toxicants., *Toxicological sciences* 57, 326-337.
12. Kochhar, S., Jacobs, D. M., Ramadan, Z., Berruex, F., Fuerholz, A., and Fay, L. B. (2006) Probing gender-specific metabolism differences in humans by nuclear magnetic resonance-based metabolomics, *Analytical Biochemistry* 352, 274-281.
13. Dieterle, F., Ross, A., Schlotterbeck, G., and Senn, H. (2006) Probabilistic quotient normalization as robust method to account for dilution of complex

- biological mixtures. Application in ^1H NMR metabonomics, *Analytical Chemistry* 78, 4281-4290.
14. Holmes, E., Nicholls, A. W., Lindon, J. C., Connon, S. C., Connelly, J. C., Haselden, J. N., Damment, S. J. P., Spraul, M., Neidig, P., and Nicholson, J. K. (2000) Chemometric models for toxicity clarification based on NMR spectra of biofluids, *Chemical Research in Toxicology* 13, 471-478.
 15. Jung, J., Park, M., Park, H. J., Shim, S. b., Cho, Y. H., Kim, J., Lee, H., Ryu, D. H., Choi, D., and Hwang, G. (2010) ^1H NMR-based metabolic profiling of naproxen-induced toxicity in rats, *Toxicology letters* 200, 1-7.
 16. Klawitter, J., Bendrick-Peart, J., Rudolph, B., Beckey, V., Klawitter, J., Haschke, M., Rivard, C., Chan, L., Leibfritz, D., Christians, U., and Schmitz, V. (2009) Urine metabolites reflect time-dependent effects of cyclosporine and sirolimus on rat kidney function, *Chemical Research in Toxicology* 22, 118-128.
 17. Lenz, E. M., Bright, J., Knight, R., Wilson, I. D., and Major, H. (2004) Cyclosporin A-induced changes in endogenous metabolites in rat urine: a metabonomic investigation using high field ^1H NMR spectroscopy, HPLC-TOF/MS and chemometrics, *Journal of Pharmaceutical and Biomedical Analysis* 35, 599-608.
 18. Nicholls, A. W., Mortishire-Smith, R. J., and Nicholson, J. K. (2003) NMR spectroscopic-based metabolomics studies of urinary metabolite variation in acclimatizing germ-free rats, *Chemical Research in Toxicology* 16, 1395-1404.

19. Tonomura, Y., Tsuchiya, N., Torii, M., and Uehara, T. (2010) Evaluation of the usefulness of urinary biomarkers for nephrotoxicity in rats, *Toxicology* 273, 53-59.
20. Williams, R. E., and Lock, E. A. (2004) D-serine-induced nephrotoxicity: possible interaction with tyrosine metabolism, *Toxicology* 201, 231-238.
21. Williams, R. E., Jacobson, M., and Lock, E. A. (2003) ¹H NMR pattern recognition and ³¹P NMR studies with D-serine in rat urine and kidney, time- and dose-related metabolic effects, *Chemical Research in Toxicology* 16, 1207-1216.
22. Williams, R. E., Major, H., Lock, E. A., Lenz, E. M., and Wilson, I. D. (2005) D-serine-induced nephrotoxicity: a HPLC-TOF/MS-based metabolomics approach, *Toxicology* 207, 179-190.
23. Yap, I. K. S., Clayton, T. A., Tang, H., Everett, J. R., Hanton, G., Provost, J. P., Le Net, J. L., Charuel, C., Lindon, J. C., and Nicholson, J. K. (2006) An integrated metabolomic approach to describe temporal metabolic dysregulation induced in the rat by the model hepatotoxin Allyl Formate, *Journal of Proteome Research* 5, 2675-2684.
24. Nicholls, A. W., Holmes, E., Lindon, J. C., Shockor, J. P., Farrant, R. D., Haselden, J. N., Damment, S. J. P., Waterfield, C. J., and Nicholson, J. K. (2001) Metabolomic investigation into Hydrazine toxicity in the rat, *Chemical Research in Toxicology* 14, 975-987.
25. Wei, L., Liao, P., Wu, H., Li, X., Pei, F., Li, W., and Wu, Y. (2009) Metabolic profiling studies on the toxicological effects of realgar in rats by ¹H NMR spectroscopy, *Toxicological and Applied Pharmacology* 234, 314-325.

26. Gao, H., Dong, B., Liu, X., Xuan, H., Houang, Y., and Lin, D. (2008) Metabonomic profiling of renal cell carcinoma: high-resolution proton nuclear magnetic resonance spectroscopy of human serum with multivariate data analysis, *Analytica Chimica Acta* 624, 269-277.
27. Gao, H., Lu, Q., Liu, X., Cong, H., Zhao, L., Wang, H., and Lin, D. (2009) Application of ¹H NMR-based metabonomics in the study of metabolic profiling of human hepatocellular carcinoma and liver cirrhosis, *Cancer Science* 100, 782-785.
28. Ng, D. J. Y., and Pasikanti, K. K. (2011) Trend analysis of metabonomics and systematic review of metabonomics-derived cancer marker metabolites, *Metabolomics* 7, 155-178.
29. Odunsi, K., Wollman, R. M., Ambrosone, C. B., Hutson, A., McCann, S. E., Tammela, J., Geisler, J. P., Miller, G., Sellers, T., Cliby, W., Qian, F., Keitz, B., Intengan, M., Lele, S., and Alderfer, J. L. (2005) Detection of epithelial ovarian cancer using ¹H-NMR-based metabonomics, *International Journal of Cancer* 113, 782-788.
30. Tiziani, S., Lopes, V., and Gunther, U. L. (2009) Early stage diagnosis of oral cancer using ¹H NMR-based metabolomics, *Neoplasia* 11, 269-276.
31. Yang, Y., Li, C., Nie, X., Feng, X., Cheng, W., Yue, Y., Tang, H., and Deng, F. (2007) Metabonomic studies of human hepatocellular carcinoma using high-resolution magic-angle spinning ¹H NMR spectroscopy in conjunction with multivariate data analysis, *Journal of proteome Research* 6, 2605-2614.

32. Kind, T., Tolstikov, V., Fiehn, O., and Weiss, R. H. (2007) A comprehensive urinary metabolomics approach for identifying kidney cancer, *Analytical Biochemistry* 363, 185-195.
33. Klawtter, J., Haschke, M., Kahle, C., Dingmann, C., Klawitter, J., Leibfritz, D., and Christians, U. (2010) Toxicodynamic effects of ciclosporin are reflected by metabolite profiles in the urine of healthy individuals after a single dose, *British Journal of Clinical Pharmacology* 70, 241-251.
34. Machtyre, D., Jimenez, B., Lewintre, E. J., Martin, C. R., Schafer, H., Ballesteros, C. G., Mayans, J. R., Spraul, M., Garcia-Conde, J., and Pineda-Lucena, A. (2010) Serum metabolome analysis by ¹H NMR reveals differences between chronic lymphocytic leukemia molecular subgroups, *Leukemia* 24, 788-797.
35. Hwang, G.-S., Yang, J.-Y., Ryu, D. H., and Kwon, T.-H. (2010) Metabolic profiling of kidney and urine in rats with lithium-induced nephrogenic diabetes insipidus by ¹H NMR-based metabonomics, *American Journal of Physiology - Renal Physiology* 298, F461-F470.
36. Holmes, E., Nicholson, J. K., and Tranter, G. (2001) Metabonomic characterization of genetic variations in toxicological and metabolic responses using probabilistic neural networks, *Chemical Research in Toxicology* 14, 182-191.
37. Bell, J. D., Sadler, P. J., Morris, V. C., and Levander, O. A. (1991) Effect of aging and diet on proton NMR-spectra of rat urine, *Magnetic Resonance in Medicine* 17, 414-422.

38. Psihogios, N. G., Gazi, I. F., Elisaf, M. S., Seferiadis, K. I., and Bairaktari, E. T. (2008) Gender-related and age-related urinalysis of healthy subjects by NMR-based metabolomics, *NMR in Biomedicine* 21, 195-207.
39. Xu, J., Yang, S., Cai, S., Dong, J., Li, X., and Chen, Z. (2010) Identification of biochemical changes in lactovegetarian urine using ¹H NMR spectroscopy and pattern recognition, *Analytical and Bioanalytical Chemistry* 396, 1451-1463.
40. Lindon, J. C., Holmes, E., and Nicholson, J. K. (2004) Toxicological applications of magnetic resonance, *Progress in Nuclear Magnetic Resonance Spectroscopy* 45, 109-143.
41. Viant, M. R., Rosenblum, E. S., and Tjeerdema, R. S. (2003) NMR-based metabolomics: a powerful approach for characterizing the effects of environmental stressors on organism health, *Environmental Science and Technology* 37, 4982-4989.
42. Lenz, E., Bright, J., Wilson, I., Morgan, S., and Nash, A. (2003) A ¹H NMR-based metabonomic study of urine and plasma samples obtained from healthy human subjects, *Journal of Pharmaceutical and Biomedical Analysis* 33, 1103-1115.
43. Lenz, E., Bright, J., Wilson, I., Hughes, A., Morrisson, J., Lindberg, H., and Lockton, A. (2004) Metabonomics, dietary influences and cultural differences: a ¹H NMR-based study of urine samples obtained from healthy British and Swedish subjects, *Journal of Pharmaceutical and Biomedical Analysis* 36, 841-849.

44. Zuppi, C., Messana, I., Forni, F., Ferrari, F., Cristina, R., and Giardina, B. (1998) Influence of feeding on metabolite excretion evidenced by urine ¹H NMR spectral profiles: a comparison between subjects living in Rome and subjects living at arctic latitudes (Svalbard), *Clinica Chimica Acta* 278, 75-79.
45. Walsh, M., Brennan, L., Malthouse, J., Roche, H., and Gibney, M. (2006) Effect of acute dietary standardization on the urinary, plasma, and salivary metabolomic profiles of healthy humans, *American Journal of Clinical Nutrition* 84, 531-539.
46. Solanky, K., Bailey, N., Beckwith-Hall, B., Bingham, S., Davis, A., Holmes, E., Nicholson, J., and Cassidy, A. (2005) Biofluid ¹H NMR-based metabonomic techniques in nutrition research - metabolic effects of dietary isoflavones in humans, *Journal of Nutritional Biochemistry*, 236-244.
47. Solanky, K., Bailey, N., Beckwith-Hall, B., Davis, A., Bingham, S., Holmes, E., Nicholson, J., and Cassidy, A. (2003) Application of biofluid ¹H nuclear magnetic resonance-based metabonomic techniques for the analysis of the biochemical effects of dietary isoflavones on human plasma profile, *Analytical Biochemistry* 323, 197-204.
48. Assfalg, M., Bertini, I., Colangiuli, D., Luchinat, C., Schafer, H., Schutz, B., and Spraul, M. (2008) Evidence of different metabolic phenotypes in humans, *Proceedings of the National Academy of Sciences of the USA* 105, 1420-1424.
49. Smilde, A., Westerhuis, J., Hoefsloot, H., Bijlsma, S., Rubingh, C., Vis, D., Jellema, R., Pijl, H., Roelfsema, F., and van der Greef, J. (2010) Dynamic metabomic data analysis: a tutorial review, *Metabolomics* 6, 3-17.

50. Carone, F. A., and Ganote, C. E. (1975) D-serine nephrotoxicity. The nature of proteinuria, glucosuria, and aminoaciduria in acute tubular necrosis, *Archives of Pathology* 99, 658-662.
51. Carone, F. A., Nakamura, S., and Goldman, B. (1985) Urinary loss of glucose, phosphate and protein by diffusion into proximal straight tubules injured by D-serine and maleic acid, *Laboratory Investigation* 52, 605-610.
52. Genote, C. E., Peterson, D. R., and Carone, F. E. (1974) The nature of D-serine-induced nephrotoxicity, *American Journal of Pathology* 77, 269-282.
53. Silbernagl, S., Volker, K., and Dantzer, W. H. (1999) D-serine is reabsorbed in rat renal pars rectal, *American Journal of Pathology* 276, F857-F863.
54. Krug, A. W., Volker, K., Dntzler, W. H., and Silbernagl, S. (2007) Why D-serine is nephrotoxic and α -aminoisobutyric acid protective? , *American Journal of Physiology - Renal Physiology* 293, F382-F390.
55. Maekawa, M., Okamura, T., Kasai, N., Hori, Y., Summer, K. H., and Konno, R. (2005) D-amino acid oxidase is involved in D-serine-induced nephrotoxicity, *Chemical Research in Toxicology* 18, 1678-1682.
56. Zanatta, A., Schuck, P. F., Viegas, C. M., Knebel, L. A., Busanello, E. N. B., Moura, A. P., and Magner, M. (2009) In vitro evidence that D-serine disturbs the citric acid cycle through inhibition of citric synthase activity in rat cerebral cortex, *Brain Research* 1298, 186-193.
57. Soto, A., DelRaso, N. J., Schlager, J. J., and Chan, V. T. (2008) D-serine exposure resulted in gene expression changes indicative of activation of fibrogenic

- pathways and down-regulation of energy metabolism and oxidative stress response, *Toxicology* 243, 177-192.
58. Spamer, E., Muller, D. G., Wessels, P. L., and Venter, J. P. (2002) Characterization of complexes of furosemide with 2-hydroxypropyl- β -cyclodextrin and sulfobutyl ether-7- β -cyclodextrin, *European Journal of Pharmaceutical Sciences* 16, 247-253.
 59. Brenner, B. M., Keimowitz, R. I., Wright, F. S., and Berliner, R. W. (1969) An inhibitory effect of furosemide on sodium reabsorption by the proximal tubule of the rat nephron. , *Journal of Clinical Investigation* 48, 290-300.
 60. Burke, T. J., Robinson, R. R., and Clapp, J. R. (1972) Determination of the effect of furosemide on the proximal tubule, *Kidney International* 1, 12-18.
 61. Christensen, S., Steiness, E., and Christensen, H. (1986) Tubular sites of Furosemide Natriuresis in volume-replaced and volume-depleted conscious rats, *The Journal of Pharmacology and Experimental Therapeutics* 239, 211-218.
 62. Seely, J. F., and Dirks, J. H. (1977) Site of action of diuretic drugs, *Kidney International* 11, 1-8.
 63. Wittner, M., Stefano, D., Wangemann, P., and Greger, R. (1991) How do loop diuretics act? , *Drugs* 41, 1-13.
 64. Hansen, L. L., Schilling, A. R., and Wiederholt, M. (1981) Effect of calcium, furosemide and chlorothiazine on net volume reabsorption and basolateral membrane potential of distal tubule, *Pflugers Archiv European Journal of Physiology* 389, 121-126.

65. Oberleithner, H., Guggino, W., and Giebisch, G. (1983) The effect of furosemide on luminal sodium, chloride and potassium transport in the early distal tubule of Amphiuma kidney. Effects of potassium adaptation, *Pflugers Archiv European Journal of Physiology* 396, 27-33.
66. Lassnigg, A., Donner, E., Grubhofer, G., Presterl, E., Druml, W., and Hiesmayr, M. (2000) Lack of renoprotective effects of dopamine and furosemide during cardiac surgery, *Journal of American Society of Nephrology* 11.
67. Brezis, M., Rosen, S., Silva, P., and Epstein, F. (1984) Transport activity modifies thick ascending limb damage in the isolated perfused kidney, *Kidney International* 25, 65-72.
68. Mahesh, B., Yim, B., Robson, D., Pillai, R., Ratnatunga, C., and Pigott, D. (2008) Does furosemide prevent renal dysfunction in high-risk cardiac surgical patients? Results of a double-blinded prospective randomised trial, *European Journal of Cardio-thoracic Surgery* 33, 370-376.
69. Costa, M., Marchetti, M., Balaszczuk, A., and Arranz, C. (2001) Effects of L-arginine and furosemide on blood pressure and renal function in volume-expanded rats, *Clinical and Experimental Pharmacology and Physiology* 28, 528-532.
70. Kutina, A. V., Zakharov, V. V., and Natochin, Y. V. (2008) Excretion of proteins by rat kidney during various types of diuresis, *Bulletin of Experimental Biology and Medicine* 146, 671-674.
71. Eilers, P. (2003) A perfect smoother, *Analytical Chemistry* 75, 3631-3636.

72. Whittaker, E. (1923) On new method of graduation, *Proceedings of the Edinburgh Mathematical Society* 41, 63-75.
73. Anderson, P. E., Mahle, D. A., Doom, T. E., Reo, N. V., DelRaso, N. J., and Raymer, M. L. (2011) Dynamic Adaptive Binning: An improved quantification technique for NMR spectroscopic data, *Metabolomics* 7, 179-190.
74. Wider, G., Baumann, R., Nagayama, K., Ernst, R. R., and Wuthrich, K. (1981) Strong spin-spin coupling in the two-dimensional J-resolved 360-MHz spectra of the common amino acids., *Journal of magnetic resonance* 42, 73-87.
75. Mahle, D. A., Anderson, P. E., DelRaso, N. J., Raymer, M. L., Neuforth, A. E., and Reo, N. V. (2010) A generalized model for metabolomics analyses: application to dose and time dependent toxicity, *Metabolomics* doi:10.1007/s11306-010-0246-3.
76. Rozman, K. K., and Doull, J. (1998) General principles of toxicology. In J. Rose (Ed.) *Environmental Toxicology: Current development*, 1-11.
77. Robertson, D. G., Ruepp, S., Stryker, S. A., Hnatyshyn, S. Y., Shipkova, P. A., Aranibar, N., Mcnaney, C. A., Fiehn, O., and Reily, M. D. (2011) Metabolomic and transcriptomic changes induced by overnight (16h) fasting in male and female Sprague-Dawley rats, *Chemical Research in Toxicology* 24, 481-487.
78. Ellis, M., Whitfield, A., Gowans, L., Auton, T., McLean Provan, W., Lock, E. A., and Smith, L. (1995) Inhibition of 4-hydroxyphenylpyruvate dioxygenase by 2-(2-nitro-4-trifluoromethylbenzoyl)-cyclohexane-1,3-dione and 2-(2-chloro-4-methanesulfonylbenzoyl)-cyclohexane-1,3-dione, *Toxicological and Applied Pharmacology* 133, 12-19.

79. Amlal, S., Chen, Q., Habo, K., Wang, Z., and Soleimani, M. (2001) Fasting downregulates renal water channel AQP2 and causes polyuria, *American Journal of Physiology, Renal Physiology* 280, F513-F523.
80. Agre, P. (2006) The aquaporin water channels, *Proceedings of the American Thoracic Society* 3, 5-13.
81. Chen, L., and Burka, L. T. (2007) Chemical and enzymatic oxidation of furosemide: formation of pyridinium salts, *Chemical Research in Toxicology* 20, 1741-1744.
82. Cvetanovic, I., Renade, V., Molnar, J., Whelton, A., and Somberg, J. (2007) The evaluation of the diuretic action of parenteral formulations of metolazone, *American Journal of Therapeutics* 14, 25-29.
83. Connor, S. C., Wu, W., Sweatman, B. C., Manini, J., Haselden, J. N., Crowther, D. J., and Waterfield, C. J. (2004) Effects of feeding and body weight loss on the ¹H-NMRbased urine metabolic profiles of male Wistar Han rats: implications for biomarker discovery, *Biomarkers* 9, 156-179.
84. Habold, C., Chevalier, C., Dunnel-Erb, S., Foltzer-Jourdainne, C., Le Maho, Y., and Lignor, J. H. (2004) Effects of fasting and refeeding on jejunal morphology and cellular activity in rats in relation to depletion of body stores, *Scandinavian Journal of Gastroenterology* 6, 531-539.
85. Kale, V. P., Joshi, G. S., Parikshit, B., and Jain, M. R. (2009) Effect of fasting duration on clinical pathology results in Wistar rats, *Veterinary Clinical Pathology* 38, 361-366.

86. Khan, A., Low, H., and Efendic, S. (1985) Effects of fasting and refeeding on the activity of hepatic glucose-6-phosphatase in rats, *Acta Physiologica Scandinavia* 124, 591-596.
87. LeBrun, M., Grenier, L., Bergeron, M. G., Thibault, L., Labrecque, G., and Beauchamp, D. (1999) Effect of fasting on temporal variation in the nephrotoxicity of Amphotericin B in rats, *Antimicrobial Agent and Chemotherapy* 43, 520-524.
88. Lenaerts, K., Sokotovic, M., Bouwman, F. G., Lamers, W. H., Mariman, E. C., and Renes, J. (2006) Starvation induces phase-specific changes in the proteome of mouse small intestine, *Journal of Proteome Research* 5, 2113-2122.
89. Boedigheimer, M., Wolfinger, R., Bass, M., Bushel, P., Chou, J., Cooper, M., Corton, J., Fostel, J., Hester, S., Lee, J., Liu, F., Liu, J., Qian, H., Quackenbush, J., Pettit, S., and Thompson, K. (2008) Sources of variation in baseline gene expression levels from toxicogenomics study control animals across multiple laboratories, *BioMed Central Genomics* 9, 285.
90. Budohoski, L., Challis, J., and Newsholme, E. (1982) Effects of starvation on the maximal activities of some glycolytic and citric acid-cycle enzymes and glutaminase in mucosa of the small intestine of the rat, *Biochemistry Journal* 206, 169-172.
91. Riis, B., Rattan, S., Clark, B., and Merrick, W. (1990) Eukaryotic protein elongation factors, *Trends in Biochemical Sciences* 15, 420-424.

92. Owens, J., Thompson, D., Shah, N., and DiGirolamo, M. (1979) Effects of fasting and refeeding in the rat adipocyte metabolic function and response to insulin, *Journal of Nutrition* 709, 1584-1591.
93. Bjorntorp, P., Enzi, G., Karlsson, M., Kral, J., Larsson, B., Sjostrom, L., and Smith, U. (1980) Effects of refeeding on adipocyte metabolism in the rat, *International Journal of Obesity* 4, 11-19.
94. Timmers, K., and Knittle, J. (1980) Effects of undernutrition and refeeding on enzyme activities and rates of glucose catabolism in rat epididymal adipose tissue, *Journal of Nutrition* 110, 1176-1184.
95. Fried, S., Hills, J., M, N., and Digirolamo, M. (1983) Prolonged Effects of Fasting-Refeeding on Rat Adipose Tissue Lipoprotein Lipase Activity: Influence of Caloric Restriction during Refeeding, *Journal of nutrition* 113, 1861-1869.
96. Bjorntorp, P., Yang, M.-U., and Greenwood, M. (1983) Refeeding after fasting in the rat: effects of carbohydrate, *American Journal of Clinical Nutrition* 37, 396-402.
97. Dimitriadis, G., Leighton, B., Parry-Billings, M., Tountas, C., Raptism, S., and Newsholme, E. A. (1998) Furosemide decreases the sensibility of glucose transport to insulin in skeletal muscle in vitro, *European Journal of Endocrinology*, 118-122.
98. Klahr, S., Yates, J., and Bourgoignie, J. (1971) Inhibition of glycolysis by ethacrynic acid and furosemide, *American Journal of Physiology* 221, 1038-1043.
99. Weller, J. M., and Borondy, M. (1967) Effect of furosemide on glucose metabolism, *Metabolism* 16, 532-536.

100. Jacobs, D., Mookerjee, B. K., and Jung, C. Y. (1984) Furosemide inhibits glucose transport in isolated rat adipocytes via direct inactivation of carrier proteins, *Journal of Clinical Investigation* 74, 1679-1685.
101. Sandstrom, P., and Sehlin, J. (1988) Furosemide-induced glucose intolerance in mice is associated with reduced insulin secretion, *European Journal of Pharmacology* 147, 403-409.
102. Jung, C. Y., and Mookerjee, B. K. (1976) Inhibitory effect of furosemide on glucose transport, *Journal of Laboratory and Clinical Medicine* 87, 960-966.
103. Myles, P., Buckland, M., Schenk, N., Cannon, G., Langley, M., BB, D., and Weeks, A. (1993) Effect of 'renal-dose' dopamine on renal function following cardiac surgery, *Anaesthesia and Intensive Care* 21, 56-61.
104. Lombardi, R., Ferreiro, A., and Servetto, C. (2003) Renal function after cardiac surgery: adverse effect of furosemide, *Renal Failure* 25, 775-786.
105. Iyalomhe, G., Omogbai, E., Ozolua, R., and Iyalomhe, O. (2008) Effects of hydrochlorothiazide and furosemide on creatinine clearance in some hypertensive Nigerians, *African Journal of Biotechnology* 7, 848-851.
106. Wise, E., and Elwyn, D. (1966) Hyperaminoaciduria in rats following D-serine administration, *Proceedings of the Society of Experimental Biology and Medicine* 121, 982-986.